JACS
JOURNAL OF THE AMERICAN CHEMICAL SOCIETY

Article

pubs.acs.org/JACS

Single-Molecule Analysis of the Supramolecular Organization of the M_2 Muscarinic Receptor and the $G\alpha_{i1}$ Protein

Rabindra V. Shivnaraine,[*,†,▽,⊗] Dennis D. Fernandes,[‡,§,⊗] Huiqiao Ji,[†,⊗] Yuchong Li,[‡,§] Brendan Kelly,[†,#] Zhenfu Zhang,[‡,§] Yi Rang Han,[†] Fei Huang,[†] Krishana S. Sankar,[∥] David N. Dubins,[†] Jonathan V. Rocheleau,[∥,⊥] James W. Wells,[*,†] and Claudiu C. Gradinaru[*,‡,§]

[†]Department of Pharmaceutical Sciences, Leslie Dan Faculty of Pharmacy, University of Toronto, Toronto, Ontario M5S 3M2, Canada

[‡]Department of Physics, University of Toronto, Toronto, Ontario M5S 1A7, Canada

[§]Department of Chemical & Physical Sciences, University of Toronto Mississauga, Mississauga, Ontario L5L 1C6, Canada

[∥]Department of Physiology, University of Toronto, Toronto, Ontario M5G 1L7, Canada

[⊥]Institute of Biomedical and Biomaterial Engineering, University of Toronto, Toronto, Ontario M5S 3G9, Canada

[#]Krembil Research Institute, University Health Network, Toronto, Ontario M5T 2S8, Canada

Supporting Information

ABSTRACT: G protein-coupled receptors constitute the largest family of transmembrane signaling proteins and the largest pool of drug targets, yet their mechanism of action remains obscure. That uncertainty relates to unresolved questions regarding the supramolecular nature of the signaling complex formed by receptor and G protein. We therefore have characterized the oligomeric status of eGFP-tagged M_2 muscarinic receptor (M_2R) and G_{i1} by single-particle photobleaching of immobilized complexes. The method was calibrated with multiplexed controls comprising 1−4 copies of fused eGFP. The photobleaching patterns of eGFP-M_2R were indicative of a tetramer and unaffected by muscarinic ligands; those of eGFP-G_{i1} were indicative of a hexamer and unaffected by GTPγS. A complex of M_2R and G_{i1} was tetrameric in both, and activation by a full agonist plus GTPγS reduced the oligomeric size of G_{i1} without affecting that of the receptor. A similar reduction was observed upon activation of eGFP-$G\alpha_{i1}$ by the receptor-mimic mastoparan plus GTPγS, and constitutively active eGFP-$G\alpha_{i1}$ was predominantly dimeric. The oligomeric nature of G_{i1} in live CHO cells was demonstrated by means of Förster resonance energy transfer and dual-color fluorescence correlation spectroscopy in studies with eGFP- and mCherry-labeled $G\alpha_{i1}$; stochastic FRET was ruled out by means of non-interacting pairs. These results suggest that the complex between M_2R and holo-G_{i1} is an octamer comprising four copies of each, and that activation is accompanied by a decrease in the oligomeric size of G_{i1}. The structural feasibility of such a complex was demonstrated in molecular dynamics simulations.

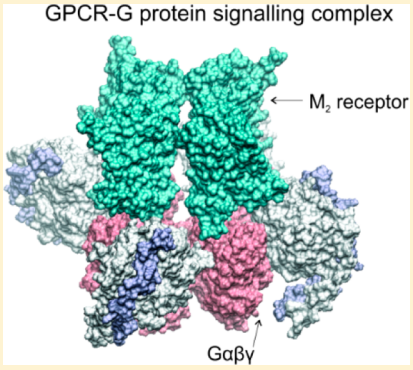

INTRODUCTION

G protein-coupled receptors (GPCRs) constitute the largest family of transmembrane proteins, with almost 4% of the protein-encoding portion of the human genome producing nearly 1000 receptors.[1] GPCRs detect a remarkably diverse set of extracellular stimuli, from photons of light to calcium, small organic molecules such as neurotransmitters and odorants, peptides, glycoproteins, and phospholipids. They occur in all organs and most tissues throughout the body,[2,3] and they regulate various intracellular processes.[4] They are implicated in many if not most diseases, and they are the targets of almost one-third of prescribed drugs.[5] In short, they are very important proteins.

All GPCRs serve as transducers of the signal between the extracellular stimulus and intracellular mediators, particularly G proteins and arrestins.[6] Binding of an agonist generally is believed to initiate the process by promoting coupling of the receptor to a guanosine diphosphate (GDP)-bound G protein.[7−10] That in turn causes the release of GDP and the formation of a stable complex between a nucleotide-free G protein and an agonist-bound receptor.[11,12] Guanosine triphosphate (GTP) then binds to the site vacated by GDP, causing the complex to dissociate into a GTP-bound G protein and an uncoupled receptor with reduced affinity for the agonist.[8,9] The release of G proteins occupied by GTP, or by a non-hydrolyzable analogue such as GTPγS, leads to downstream signaling.[13] This general understanding has fostered a view of receptors as simple on−off switches, but that now seems simplistic. More recent evidence for multiple active states

Received: April 26, 2016
Published: August 5, 2016

DOI: 10.1021/jacs.6b04032
J. Am. Chem. Soc. 2016, 138, 11583−11598

of the receptor and preorganized signaling units has pointed to greater complexity and prompted a reexamination of prevailing theories and models.[14]

Adding to this complexity, we have shown that GTP-induced changes in the affinity of agonists for muscarinic receptors in myocardial membranes differ from those predicted for transient complexes of monomeric receptors and G proteins.[9] In a comparison of purified M_2 muscarinic receptors reconstituted as monomers in size-selective nanodiscs and as tetramers in phospholipid vesicles, we demonstrated that only the latter reproduce the effects of guanylyl nucleotides on the receptor in sarcolemmal preparations.[15] Moreover, cooperative interactions between the constituent protomers of an oligomer can account for ligand-binding properties that otherwise are difficult to explain,[8] and they have been shown to underlie the functioning of GPCRs of Family C such as the metabotropic glutamate and GABA receptors.[16] Dimers or larger oligomers of the M_2 and M_3 muscarinic receptors have been identified directly through biochemical approaches, such as co-immunoprecipitation[17] and chemical cross-linking,[18] and in biophysical studies based on bioluminescence and Förster resonance energy transfer (BRET[19] and FRET[20]). There has been no direct measurement of the oligomeric status of a GPCR or its associated G protein when coupled in a signaling complex.

The role served by oligomers of GPCRs has been a subject of much debate. The controversy is due in part to questions regarding the design and interpretation of studies based on BRET.[21,22] Also, measurements of single-molecule fluorescence have identified a preponderance of monomers in some studies[23,24] and of dimers in others.[25,26] Such differences in the oligomeric state may be due to differences among different receptors, in the preparation of samples, or in the interpretation of data. FRET-based attempts to estimate the oligomeric size of a GPCR upon activation by agonists similarly have led to mixed results, with an increase[27] in one case and little or no change in others.[20,28] Challenges typically faced in such experiments include uncertainty over what fraction of the total number of receptors is being measured and the difficulty detecting and accounting for mixtures of oligomers of different size.

Approaches based on single-molecule fluorescence, such as single-molecule photobleaching (smPB), provide a direct measure of the oligomeric size of individual particles and therefore give access to the distribution of oligomeric sizes across the full ensemble. Such experiments typically involve the immobilization of individual protein complexes in which each protomer is tagged with a single fluorophore. The oligomeric size of each complex then is inferred from the number of stepwise drops in the trace of fluorescence intensity over time.[29−31] In this study, we charecterized the oligomeric states of the M_2 receptor and the G_{i1} protein, both separately and coupled together in a complex. To obtain the required probes, enhanced green fluorescent protein (eGFP) was fused to the N-terminus of the human M_2 muscarinic cholinergic receptor, inserted in the $G\alpha_{i1}$-subunit, or fused to the N-terminus of the $G\gamma_2$-subunit. The signal was calibrated using fused multimers of eGFP of known oligomeric size, purified to homogeneity.

Distributions of the number of photobleaching steps were acquired for the receptor and G_{i1} at different stages of the signaling process, which were attained by treatment of the immobilized particles with agonists, antagonists, and guanylyl nucleotides. The results of photobleaching (PB) *in vitro* were complemented *in vivo* by dual-color fluorescence correlation spectroscopy (dcFCS) and quantitative FRET, which were used to identify and characterize oligomers of eGFP- and mCherry (mCh)-tagged G_{i1} in live CHO cells. The spectroscopic data describe a supramolecular complex comprising an oligomer of the M_2 receptor on the one hand and of G_{i1} on the other, and the spatial feasibility of such a complex was demonstrated in molecular dynamics simulations.

RESULTS

Functionality of Tagged G Proteins and Receptors. Human $G\alpha_{i1}$ and heterotrimeric $G\alpha_{i1}\beta_1\gamma_2$ were extracted in GDP-free form from *Sf*9 cells as described in the Supporting Information (SI), Section S1. $G\alpha_{i1}$ was modified by the insertion of hexahistidine (His_6), eGFP, mCherry (mCh), or combinations thereof between positions 91 and 92 to form His_6-$G\alpha_{i1}$, eGFP-$G\alpha_{i1}$, His_6-eGFP-$G\alpha_{i1}$, mCh-$G\alpha_{i1}$, and His_6-mCh-$G\alpha_{i1}$ (Figure 1A,B). The functionality of purified His_6-$G\alpha_{i1}$ was confirmed by changes in the emission intensity of tryptophan 211, which is sensitive to conformational movements in switch region II.[32] The intensity decreased upon the addition of 10 μM GDP and increased upon the subsequent addition of 10 mM AlF_4^- (Figure S1D−F).

The insertion of a fluorescent protein with or without His_6 did not disrupt the formation of holo-G_{i1} from $G\alpha_{i1}$ and $G\beta_1\gamma_2$ or interfere with the binding of [^{35}S]GTPγS. When mCh-$G\alpha_{i1}$ and eGFP-$G\beta_1\gamma_2$ were co-expressed in CHO cells and monitored by dcFCS (Figure 1D), the amplitudes of the auto- and cross-correlation curves indicated that 91% of the limiting species—in this case, mCh-$G\alpha_{i1}$—migrated as a heterotrimer (Figure 1D, inset). There was little or no cross-correlation with a negative control in which mCh-$G\alpha_{i1}$ was co-expressed with a fusion protein comprising the first 30 amino acids of $G\alpha_{i1}$ (MP) and eGFP (i.e., MP-eGFP) (Figure 1D, inset). The MP sequence contains the sites of myristoylation and palmitoylation in $G\alpha_{i1}$[33] and is responsible for its localization at the plasma membrane (Figure 2D, inset). In binding studies on His_6-tagged $G\alpha_{i1}$ and $G\alpha_{i1}\beta_1\gamma_2$ purified by chelating chromatography, the affinity of [^{35}S]GTPγS was similar or the same irrespective of the presence of eGFP (His_6-$G\alpha_{i1}$, log K = −5.66; His_6-eGFP-$G\alpha_{i1}$, log K = −6.26) or of $G\beta\gamma$ (eGFP-$G\alpha_{i1}\beta_1$-His_6-γ_2, log K = −6.01) (Figure 1E, Table S1).

Human M_2 muscarinic receptor fused at the N-terminus to eGFP (eGFP-M_2)[20] or at the C-terminus to mCherry (M_2-mCh) was extracted from *Sf*9 or CHO cells in digitonin−cholate as described previously.[34,35] The affinity of *N*-[^{3}H]methylscopolamine ([^{3}H]NMS) was indistinguishable in assays on the wild-type receptor and both fluorophore-tagged mutants (log K = −8.01 ± 0.12, eq 6 with n_H = 1, N = 4). A fused fluorescent protein therefore did not affect the ability of the receptor to bind the radiolabeled antagonist, as reported previously.[20]

Purification of a Receptor-G Protein Complex. Complexes of the M_2 receptor and $G\alpha_{i1}$ or heterotrimeric G_{i1} were purified from membranes of CHO cells and *Sf*9 cells as described in the SI, Section S1. In each case, the complex was stabilized by the inclusion of carbachol before and during purification and by the enzyme-assisted removal GDP from the G protein using a strategy described previously.[36]

Coupling of co-purified receptors and G proteins was confirmed by FRET within a complex of eGFP-tagged $G\alpha_{i1}$ (eGFP-$G\alpha_{i1}$) and the M_2 receptor fused at its C-terminus to mCherry (M_2-mCh). Excitation of eGFP at 488 nm resulted in an emission spectrum with a peak at 610 nm, which arises from

DOI: 10.1021/jacs.6b04032
J. Am. Chem. Soc. 2016, 138, 11583−11598

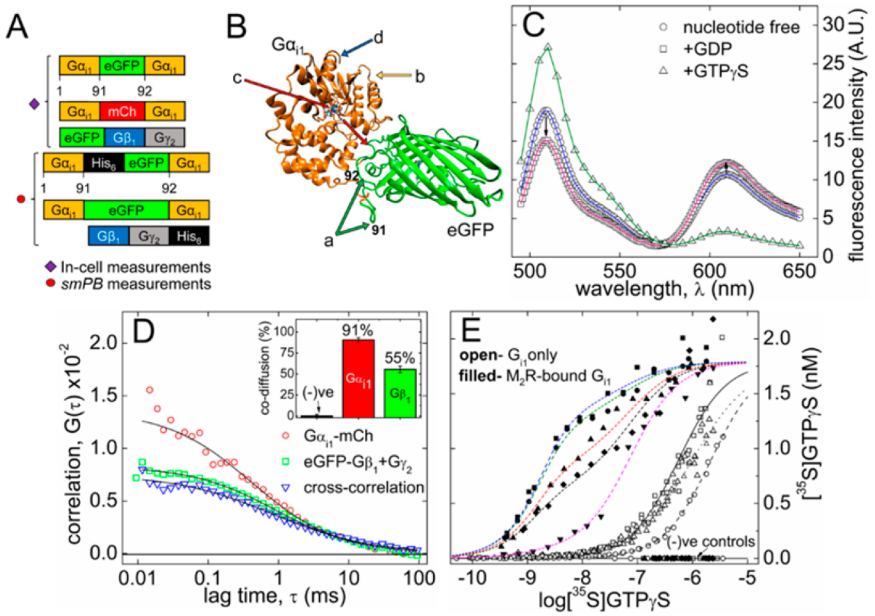

Figure 1. Structure and functionality of tagged $G\alpha_{i1}$. (A) For measurements in live cells, eGFP or mCherry was inserted at position 91 of $G\alpha_{i1}$, and eGFP was fused to the N-terminus of $G\beta_1$. For measurements of immobilized single particles, His_6-eGFP and eGFP were inserted at position 91 of $G\alpha_{i1}$, and His_6 was fused to the N-terminus of $G\gamma_2$. (B) A molecular model of eGFP-$G\alpha_{i1}$ was rendered from the crystallographic structures of $G\alpha_{i1}$ (PDB ID: 1GIA)[50] and GFP (PDB ID: 2WUR).[76] Regions of interest are indicated by arrows as follows: point of insertion (a, green), binding locus of $G\beta\gamma$ (b, yellow), pathway for binding and release of guanylyl nucleotides (c, red), and binding locus of the receptor (d, blue). (C) Samples of M_2-mCh and His_6-eGFP-$G\alpha_{i1}$ copurified as a complex from CHO cells were excited at 488 nm, and the emission spectrum was recorded in the absence of guanylyl nucleotide (○, blue) and in the presence of GDP (10 μM) (□, red) or GTPγS (10 μM) (△, green). The solid lines are the fits to the data of a linear superposition of the emission spectra of eGFP and mCherry (eq 3). FRET was increased by the inclusion of GDP, as indicated by the decrease in emission at 507 nm and the increase at 610 nm (arrows), and it was almost eliminated by the inclusion of GTPγS. (D) Fluorophore-tagged $G\alpha_{i1}$ was co-expressed with $G\beta_1$ and $G\gamma_2$ in CHO cells and monitored by dcFCS; intensity autocorrelation of mCh-$G\alpha_{i1}$ (○, red) and eGFP-$G\beta_2$ (□, green), cross-correlation (▽, blue). The lines represent the best fits of eq 1 (only diffusion components are shown) or eq 2. The fractions of co-diffusing species are shown in the inset, where the negative control (−ve) is the higher of the two values obtained with MP-eGFP and mCh-$G\alpha_{i1}$ plus $G\beta_1\gamma_2$. (E) Binding of [^{35}S]GTPγS to $G\alpha_{i1}$ or holo-G_{i1} expressed alone (open symbols) or together with M_2 receptor (filled symbols) in *Sf*9 cells and purified by chelating chromatography; His_6-$G\alpha_{i1}$ (○), His_6-eGFP-$G\alpha_{i1}$ (△), eGFP-$G\alpha_{i1}\beta_1$-His_6-γ_2 (□), M_2−eGFP-$G\alpha_{i1}\beta_1$-His_6-γ_2. Different closed symbols (●, ■, ▲, ▼, ◆) denote data from different experiments. The lines represent the best fits of eq 6, and the parametric values are listed in Table S1.

the non-radiative transfer of energy (FRET) from the donor (eGFP) to the acceptor (mCherry) (Figure 1C). The spectrum was unmixed to obtain the contribution of each fluorophore (eGFP, k_D; mCherry, k_A) (eq 3) and the corresponding estimate of the apparent FRET efficiency (E_{app}, eq 4), which was about 70% with $G\alpha_{i1}$ in the nucleotide-free state and increased to about 78% in the presence of 10 μM GDP. FRET was lost upon the addition of 10 μM GTPγS (Figure 1C), which virtually eliminated the peak at 610 nm and reduced E_{app} essentially to zero. The effects of GDP and GTPγS suggest that the purified complex retained native functionality, and the effect of GTPγS is consistent with uncoupling of the G protein from the receptor.

The functionality of a purified complex of the M_2 receptor and heterotrimeric G_{i1} (i.e., M_2-eGFP-$G\alpha_{i1}\beta_1$-His_6-γ_2) was demonstrated in the binding of [^{35}S]GTPγS, which revealed marked heterogeneity (Figure 1E, closed symbols). Two classes of sites are required to describe binding to receptor-coupled $G\alpha_{i1}$ (eq 6), whereas one class is sufficient for all forms of $G\alpha_{i1}$ purified in the absence of receptor (i.e., His_6-$G\alpha_{i1}$, His_6-eGFP-$G\alpha_{i1}$, and eGFP-$G\alpha_{i1}\beta_1$-His_6-γ_2) (Table S1). Both affinities of the complex ($\log K_1 = -9.03 \pm 0.04$, $\log K_2 = -7.13 \pm 0.04$) are at least 7.4-fold higher than the single affinity of receptor-free $G\alpha_{i1}$ or $G\alpha_{i1}\beta_1\gamma_2$ ($\log K = -6.26$ to -5.66). Because the purification was based on His_6-tagged $G\gamma_2$, the absence of low-affinity sites in preparations of M_2-eGFP-$G\alpha_{i1}\beta_1$-His_6-γ_2 indicates that all $G\alpha_{i1}$ in the purified complex was coupled to M_2 receptor.

The M_2 receptor therefore appears to impart heterogeneity within a population of G proteins that otherwise is functionally homogeneous. Also, different preparations of the purified complex differed markedly in the apparent distribution of sites between the two states revealed by [^{35}]GTPγS (Figure 1E). Global analysis of the biphasic binding patterns using eq 6 indicates that the values of $\log K_1$ and $\log K_2$ can be shared among the different curves ($P > 0.5$), whereas each curve requires a separate value for the fraction of sites ostensibly in one state or the other (F_j) (Table S1).

Oligomers of G Proteins in Live Cells. eGFP- and mCherry-tagged $G\alpha_{i1}$ were co-expressed together with $G\beta_1\gamma_2$ in CHO cells, and oligomers of G_{i1} were detected at the cell membrane by dcFCS and FRET (Figure 2). Intensity autocorrelation curves from dcFCS had similar amplitudes for eGFP and mCherry, indicating that the two fluorescent proteins were expressed at similar levels (N_i, eq 1) (Figure 2A). A comparison of those values with the amplitude of the cross-correlation curve suggests that about 50% of each diffusing α_{i1}-subunit migrated as a complex that contained both tags (N_x, eq 2) (Figure 2A, inset).

It has been reported previously that cross-correlation amplitudes can be affected by spectral cross-talk[37] and by PB and maturation of the fluorophores.[38] In our experiments, only

DOI: 10.1021/jacs.6b04032
J. Am. Chem. Soc. 2016, 138, 11583−11598

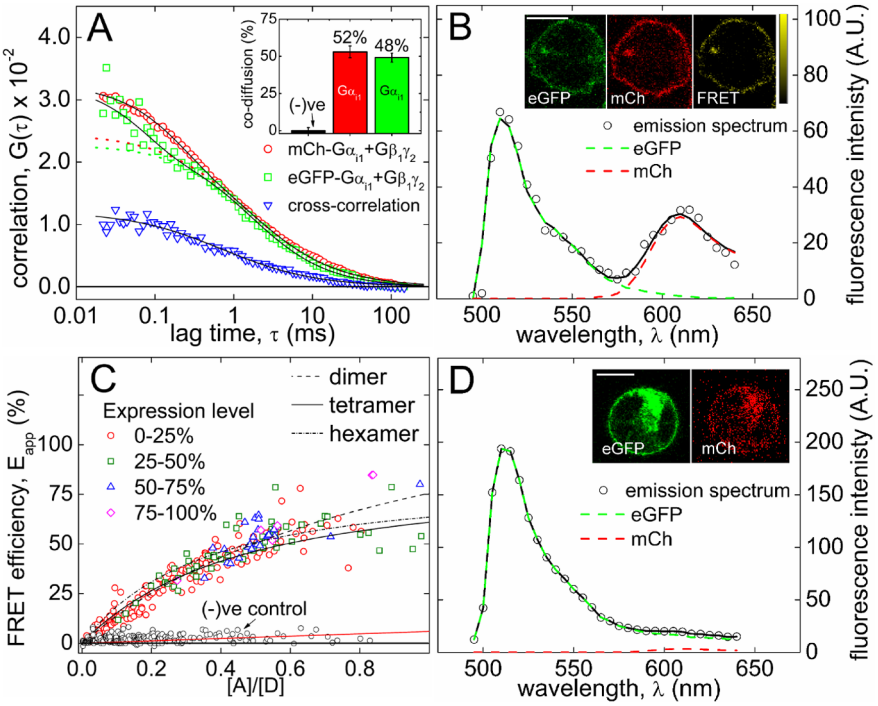

Figure 2. Oligomers of G_{i1} in live cells. eGFP-Gα_{i1} and mCh-Gα_{i1} were co-expressed together with G$\beta_1\gamma_2$ in CHO cells and monitored by dcFCS and FRET. (A) Correlation curves from cells transfected with equal amounts of DNA coding for eGFP-Gα_{i1} and mCh-Gα_{i1}; autocorrelation of eGFP-Gα_{i1} (○, green) and mCh-Gα_{i1} (□, red), and cross-correlation (▽, blue). The solid lines represent the best fits of eqs 1 and 2, and the dotted lines indicate the contribution of diffusing species. The fractions of co-diffusing species are shown in the inset, where the negative control (−ve) is the higher of the two values obtained with MP-eGFP and mCh-Gα_{i1} plus G$\beta_1\gamma_2$. (B) Confocal imaging of CHO cells co-expressing eGFP-Gα_{i1} and mCh-Gα_{i1}. Cells were excited at 488 nm, and the measured emission spectrum from the region of the membrane of a typical cell is shown in the figure (○). The spectrum was unmixed as described in the SI, Section S2 (eq 3), to obtain the fitted spectrum (black) and the individual contributions of donor (eGFP, green) and acceptor (mCh, red). Images of the cell are shown in the insets, from left to right: emission from the donor upon excitation at 488 nm, emission from the acceptor upon excitation at 543 nm, FRET efficiency. The efficiency was approximated as the ratio of emission intensities corresponding to the acceptor (585−640 nm) and the donor (495−585 nm) from single pixels upon excitation at 488 nm. Distance scale bar, 10 μm; FRET scale bar, 0−100%. (C) Apparent FRET efficiencies (E_{app}) were calculated according to eq 4 for individual CHO cells co-expressing eGFP-Gα_{i1} and mCh-Gα_{i1} (colored symbols) at different levels of total Gα_{i1} (i.e., eGFP-Gα_{i1} + mCh-Gα_{i1}) and different ratios of acceptor to donor ([A]/[D]). The amounts of mCh-Gα_{i1} ([A]) and eGFP-Gα_{i1} ([D]) were determined from the fluorescence intensities of membranes upon excitation at 488 and 543 nm (SI, eqs S2 and S3), respectively. All cells are divided equally into four groups based on total Gα_{i1} (○, red, lowest quartile; ◊, purple, highest quartile). The black lines represent the best fits of eq 5 with n taken as 2 (---, 4 (—), or 6 (-·-), and the fitted values of the pairwise FRET efficiency (E_p) are listed in Table S2. Cells co-expressing MP-eGFP and mCh-Gα_{i1} at similar levels were used to test for stochastic FRET (black symbols, − ve control), and the values of E_{app} were obtained as described above for cells expressing eGFP-Gα_{i1} and mCh-Gα_{i1}. The solid red line is the best fit of a straight line. (D) Confocal imaging of CHO cells co-expressing MP-eGFP and mCh-Gα_{i1}. The data were acquired and processed as described for panel B. FRET was negligible, and the corresponding image is not shown.

about 4% of the emission from eGFP leaked into the mCherry channel, where it contributed at most 10% of the signal; thus, any contribution of spectral cross-talk to the cross-correlation curve was negligible. The laser excitation intensities were comparable to those used previously in FCS studies of GPCRs,[39] suggesting that PB also was negligible, and the fitted model accounts explicitly for triplet states of eGFP and mCherry (eq 1). It has been estimated that only 40−50% of mCherry expressed in live cells is fluorescent, and a population of dark fluorophores leads to a corresponding reduction in the amplitude of the cross-correlation curve.[38] The fraction of co-diffusing species estimated by dcFCS therefore can be regarded as a lower limit. Taken together, the co-migration of eGFP-Gα_{i1} with mCh-Gα_{i1} (Figure 2A) and that of mCh-Gα_{i1} with eGFP-G$\beta_1\gamma_2$ (Figure 1D) indicate that oligomers account for a large fraction of heterotrimeric G_{i1} in live cells.

The size of oligomers detected by dcFCS can be roughly estimated from the molecular brightness of eGFP-Gα_{i1}. The number of molecules of eGFP-G$\alpha_{i1}\beta_1\gamma_2$ in the detection volume of the cell illustrated in Figure 2A was 33 (N_g, eq 1), which corresponds to a molecular brightness of 1.5 kcps/molecule. The molecular brightness averaged over 20 cells was 1.7 ± 1 kcps/molecule. In contrast, the molecular brightness of membrane-localized eGFP (i.e., MP-eGFP) averaged over 10 cells was 0.8 ± 2 kcps/molecule. G proteins therefore appeared to be approximately twice as bright as the monomeric control, suggesting that they occurred in pairs. Because eGFP-Gα_{i1} was co-expressed with mCh-Gα_{i1}, the true oligomeric size very likely exceeded 2. The comparatively large standard deviation on the estimate of the molecular brightness may arise from variations in the oligomeric size or from variations in the complement of eGFP- and mCherry-labeled Gα_{i1} among different complexes.

Oligomers also were detected in spectrally resolved confocal images, which revealed FRET between eGFP-Gα_{i1} and mCh-Gα_{i1}. Both fluorophores were localized at the plasma membrane (Figure 2B, inset), where emission spectra recorded upon excitation of the donor (eGFP, λ_{ex} = 488 nm) included a peak arising from the acceptor (mCherry, λ_{max} = 610 nm) (Figure 2B). Spectra from individual cells were unmixed (eq 3),

DOI: 10.1021/jacs.6b04032
J. Am. Chem. Soc. 2016, 138, 11583−11598

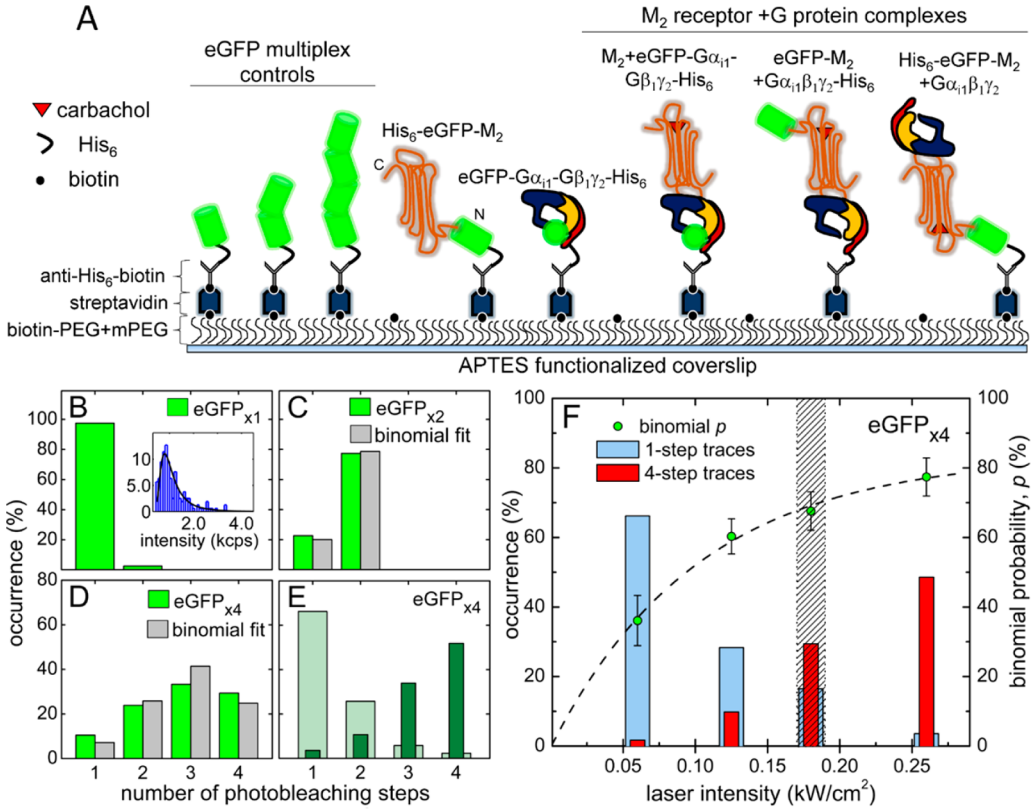

Figure 3. Immobilization of single particles and photobleaching of multiplexed eGFP. (A) Single molecules of $eGFP_{xj}$ (j = 1, 2, and 4) or single complexes of M_2 receptor (brown), holo-G_{i1} (α_{i1}, blue; β_1, yellow; γ_2, red), or both were attached to surfaces prepared by successive layering of streptavidin and biotinylated anti-His antibody on a surface coated with sparsely biotinylated PEG. (B–D) Sparsely immobilized particles of $eGFP_{xj}$ were excited at 473 nm and an intensity of 180 W/cm^2 to produce the histograms of photobleaching steps (green bars) shown for $eGFP_{x1}$ (B), $eGFP_{x2}$ (C), and $eGFP_{x4}$ (D). The gray bars in panels C and D show the best fit to eq 7 (n = 2 and 4, respectively). The fitted parametric values and the corresponding statistical counting errors are listed in Table S3. The inset to panel B shows the distribution of intensities defined by the amplitudes of the single steps in the intensity–time traces; the line represents the best fit of eq 8, and the fitted value of μ is 1243 ± 52 (Table S3). (E) smPB distributions for $eGFP_{x4}$ were also measured at a power of ~60 W/cm^2 (light green bars) and ~260 W/cm^2 (dark green bars). (F) The probability of excitation and detection (p) and the percentage occurrence of one-step traces (blue bars) and four-step photobleaching traces (red bars) are shown for $eGFP_{x4}$ for different excitation intensities. The values of fitted p (eq 7) and accompanying errors are the mean and standard deviation, respectively, from three independent measurements. The shaded region indicates the range of excitation intensity used in all experiments on the M_2 receptor and G_{i1}, except when stated otherwise. The dashed line represents the best fit from an empirical analysis of p in terms of a single-exponential rise.

and the contributions of donor (k_D) and acceptor (k_A) were used to calculate the apparent FRET efficiency for each cell (E_{app}, eq 4). The values of E_{app} and the corresponding ratios of acceptor to donor ([A]/[D]), which were estimated from the spectral properties (SI, eqs S2 and S3), are plotted in Figure 2C. Differences in the levels of expressed eGFP-Gα_{i1} and mCh-Gα_{i1} were achieved by varying the amounts of transfected plasmids and occurred stochastically within each population of transfected cells.

The apparent FRET efficiency increased with [A]/[D] up to a maximum of 50–75% in a manner that was independent of the total amount of Gα_{i1}, which varied 64-fold among 279 cells (Figure 2C). The data were fitted by eq 5[20,40] to obtain the pairwise efficiency (E_p) for FRET between a single donor and a single acceptor in an oligomer of specified size n. The value of 151% obtained for E_p in a dimer (n = 2) exceeds the theoretical limit of 100%, and the value of 91% obtained for a trimer (n = 3) is unrealistically high. A reasonable transfer efficiency of 67% was obtained for a tetramer (n = 4), and larger oligomers yielded progressively smaller values of E_p (Table S2). These considerations suggest that the complexes formed by G_{i1} at the plasma membrane of live CHO cells are trimeric or larger, at least according to the model described by eq 5 and in agreement with the molecular brightness of the complex detected by dcFCS. Essentially the same results were obtained with cells co-expressing G_{i1}, Gβ_1, Gγ_2, and the M_2 receptor, both in the absence of ligand and in the presence of the agonist carbachol (10 mM).

Measurements on the membrane-bound control (MP-eGFP) indicated that effects detected with eGFP- and mCherry-tagged Gα_{i1} were not a consequence of stochastic interactions. Co-expressed MP-eGFP and mCh-Gα_{i1} were co-localized at the plasma membrane (Figure 2D, inset), but the peak at 610 nm was absent (Figure 2D); also, the value of E_{app} was essentially independent of the relative amounts of donor and acceptor and never exceeded 5% (Figure 2C). Levels of expression in experiments with the control were comparable to those in experiments with eGFP-Gα_{i1} and mCh-Gα_{i1}. In a representative sample of cells expressing the control as donor (N = 52), the densities calculated from the spectral properties (SI, Section S2) were 3739–13 200 molecules/μm^2 for MP-eGFP and 2506–11 160 molecules/μm^2 for mCh-Gα_{i1}; the total density was 6244–24 360 molecules/μm^2 (mean ± SD, 11 460 ± 3239 molecules/μm^2). In a sample of cells expressing Gα_{i1} as donor

DOI: 10.1021/jacs.6b04032
J. Am. Chem. Soc. 2016, 138, 11583–11598

(N = 74), the densities were 1578−34 730 molecules/μm^2 for eGFP-Gα_{i1} and 1391−15 450 molecules/μm^2 for mCh-Gα_{i1}; the total density was 4557−43 960 molecules/μm^2 (mean ± SD, 14 920 ± 8473 molecules/μm^2).

The absence of FRET with the negative control is consistent with the failure of MP-eGFP to co-migrate with mCh-Gα_{i1} during dcFCS (Figure 2A, inset). In the latter experiments, the local concentration of fluorophores in the cell membrane was 50−5000 molecules/μm^2. That approaches the lower end of the range estimated from the confocal images (6244−24 360 molecules/μm^2), and the levels of expression therefore were comparable in the two assays. The average intermolecular distance between fluorophores at a concentration of 5000 molecules/μm^2 is 14 nm, which is 2.9-fold greater than the Förster radius of 4.86 nm for eGFP and mCherry (SI, Section S2). Even at an average intermolecular distance of only 7 nm (equivalent to 20 000 molecules/μm^2), the theoretical FRET efficiency of 10% is markedly lower than the value of 50−75% measured at high ratios of acceptor to donor (Figure 2C).

Complexes of Gα_{i1} identified by dcFCS and FRET do not appear to be an artifact of overexpression. A value of 1.7 × 10^6 molecules per cell has been reported for M_2 muscarinic receptors at the plasma membrane of intact cardiomyocytes from rat atria.[41] This places a lower limit on the number of accessible G proteins, which equals or exceeds the number of M_2 receptors in sarcolemmal membranes from porcine atria.[42] The surface area of CHO cells is about 600 μm^2, assuming a sphere with a diameter of 14 μm.[43] The density of 50−5000 molecules/μm^2 estimated for Gα_{i1} by dcFCS therefore is equivalent to 30 000 to 3 × 10^6 molecules per cell; the density of 4557−43 960 molecules/μm^2 estimated from the spectral properties equates to 2.7−26 × 10^6 molecules per cell. These considerations suggest that Gα_{i1} in most transfected CHO cells was expressed at levels similar to those in heart cells. Also, CHO cells were transfected under conditions similar to those used previously in studies of fluorophore-tagged M_2 receptors, which were quantified by means of a radiolabeled antagonist.[20] The measured density of 0.88 × 10^6 receptors per CHO cell was about 50% of that reported for M_2 receptors on the surface of cardiomyocytes; similarly, the density of 1.5 nmol of receptor per gram of total protein in CHO cells was about 40% of that in porcine sarcolemmal membranes. Such numbers indicate that the quantities of M_2 receptor and Gα_{i1} in transfected CHO cells are not necessarily atypical, at least when compared to those in myocardial tissue.

The foregoing considerations suggest that FRET between the fluorophore-tagged α-subunits of G_{i1} arose from interactions between heterotrimeric G proteins within a biologically relevant oligomer. The failure of a 64-fold change in the amount of total Gα_{i1} to affect the dependence of E_{app} on the ratio of acceptor to donor indicates that the size and prevalence of those oligomers is constant, at least under the conditions of the assays. Because the amount of Gα_{i1} in untransfected CHO cells was below the level of detection and negligible compared to that of transfected Gα_{i1}, as determined by Western blotting (Figure S1B,C), it seems unlikely that FRET and the results of dcFCS are affected by endogenous G proteins.

Photobleaching of Multiplexed eGFP. The oligomerization state of eGFP-tagged M_2 receptor and G_{i1} was characterized further by smPB. To establish the relationship between the number of smPB steps and oligomeric size, multiplexes of eGFP were prepared in which one, two, and four units of the fluorophore were fused head-to-tail with a single hexahistidyl tag at the N-terminus (i.e., eGFP$_{xj}$, where j = 1, 2, or 4) (Figure 3A and Figure S2A). Each multiplex was purified from *E. coli* (SI, Section S1), and the homogeneity and multimeric status were confirmed by Western blotting with a monoclonal antibody against eGFP (Figure S2B).

Sparsely immobilized particles of eGFP$_{xj}$ were irradiated at 473 nm and ∼180 W/cm^2 under a TIRF microscope, and the fluorescence intensities were recorded over time. The stepwise PB transitions displayed by each particle were identified by a change-point algorithm (SI, Section S4), and histograms of the number of PB steps obtained for eGFP$_{x1}$, eGFP$_{x2}$, and eGFP$_{x4}$ are shown in Figure 3B−D.

Almost without exception, the maximum number of PB steps was less than or equal to the number of fluorophores within the multiplex. For instance, 97% of the fluorescent spots in images of eGFP$_{x1}$ showed a single PB step, and the remaining 3% showed two PB steps. Similarly, particles of immobilized eGFP$_{x2}$ showed one or two PB steps, and those of immobilized eGFP$_{x4}$ showed 1−4 PB steps; no particle displayed more than two or four PB steps, respectively. Equivalence between the maximum number of PB steps and the number of fused fluorophores indicates that there was little or no colocalization of eGFP$_{x1}$ or its multiplexed congeners. The absence of PB steps in excess of those expected of a single molecule of eGFP$_{xj}$ is consistent with the low average density of immobilized particles, which was 0.01−0.10 per μm^2 with eGFP$_{xj}$ and the various complexes of receptor and G protein described below. A density of 0.10 μm^{-2} corresponds to a mean distance between particles of about 3 μm.

In accord with the limit on the number of PB steps, the step-histograms are well described by the binomial distribution with n taken as the number of fused eGFPs (eq 7, Figure 3C,D). Larger or smaller values of n gave diminished agreement (Figure S3H). The intensities of the single PB steps observed with eGFP$_{x1}$ were distributed in a skewed Gaussian-like manner (Figure 3B, inset), and similar intensity distributions were obtained for each PB step in the traces recorded for eGFP$_{x2}$ and eGFP$_{x4}$. The most likely step size was similar throughout, as indicated by the similar values of μ obtained from analyses in terms of the generalized extreme value (GEV) distribution (eq 8) (Table S3).

Agreement between the smPB histograms and the binomial distribution allows for the calculation of a probability (p) that an individual fluorophore within the multiplex will be photoactive. That probability relates to the photophysics of excitation and emission, the photo-viability of the sample, the threshold of detection, or all of the above. To examine this relationship, eGFP$_{x4}$ was excited at different intensities from 60 to 260 W/cm^2. At the lowest power, the smPB histogram was dominated by traces containing one and two steps, whereas at the highest power, three- and four-step traces were predominant (Figure 3E). In terms of the binomial model, the probability of occurrence of the fourth PB step increased from 2% at 60 W/cm^2 to about 50% at 260 W/cm^2 (Figure 3F). This sensitivity to the excitation power suggests that the value of p is determined by the chance of exciting a single fluorophore within the multiplex and detecting a smPB event within a noisy trace (SI, Section S4).[44,45] There also may be a minor fraction of eGFPs that cannot fluoresce owing to pre-bleaching, misfolding, or incomplete maturation of the fluorophore. Such dark elements may account for some particles with fewer than n PB steps and for the apparent

DOI: 10.1021/jacs.6b04032
J. Am. Chem. Soc. 2016, 138, 11583−11598

limit of 80−90% on p at higher laser power (Figure 3F and Table S3).

These observations indicate that a multiplexed fluorophore such as $eGFP_{xj}$ or a homogeneous population of stoichiometrically tagged homo-oligomers will yield a distribution of PB steps in which the maximum number of steps is the same as the size of the oligomer. The measurements of eGFP-tagged receptors and G proteins described below were taken at an intermediate laser power of 150−180 W/cm^2. That proved sufficient to excite multiple units of eGFP within a complex while limiting their simultaneous or premature PB and avoiding traces of short duration or low signal-to-noise ratios (SI, Section S4).

Photobleaching of the M_2 Receptor. M_2 receptor fused at the N-terminus to eGFP was purified and immobilized via a hexahistidyl tag on the fluorophore (His_6-eGFP-M_2, Figure 3A). The intensity traces of individual particles in TIRF images displayed up to six PB steps (Figure 4A), with ∼80% of the particles showing more than two steps (Table S3). The distribution of the number of PB steps is consistent with the binomial distribution (eq 7) with n taken as 6 (Figure 4A). The fitted value of p from the binomial distribution (i.e., 59.4%) corresponds to an average of 3.6 PB steps per particle (i.e., $N_{avg} = np$) (Table S3).

The distribution of intensities for each PB step from 1 through 4 resembles the skewed distributions from controls of multiplexed eGFP (Figure 4B, Table S3), suggesting that each of the first four PB steps in traces from the receptor corresponds to a single eGFP. In contrast, the distributions of intensities for PB steps 5 and 6 do not resemble those of the eGFP controls and could not be described by the GEV distribution (Figure 4B). Such anomalous behavior may arise from fluorescent impurities, which are known to bleach faster than the photostable fluorophores used in single-molecule studies.[46] They therefore would appear as higher-indexed events in the intensity−time trace, where the PB steps are numbered from right to left (Figure S3G). Also, the same anomalies were absent from particles of $eGFP_{xj}$ and eGFP-G_{i1}, as described below, suggesting that they were linked in some way to the receptor or to differences between samples purified from *E. coli* on the one hand and *Sf*9 cells on the other. Although the origin of steps 5 and 6 is unclear, the patterns displayed by steps 1−4 are indicative of particles with four fluorophores, such as a tetramer.

Muscarinic ligands had little or no effect on the distribution of PB steps (cf. Figure 4A,C). The value of N_{avg} calculated for the vacant receptor from the fitted estimate of p (eq 7, $n = 6$) is 3.6 (Table S3); the corresponding values for the receptor plus the agonist carbachol and the inverse agonist NMS are 3.43 and 3.27, respectively, at a saturating concentration of each ligand (Table 1). Similarly, the distributions of PB intensities obtained with liganded receptors resembled those of the vacant receptor, including the anomalous behavior of steps 5 and 6. The distribution shown in Figure 4A was obtained in the absence of a reducing agent, but essentially the same pattern was obtained in the presence of 10 mM DTT. This latter observation and the results from multiplexed controls suggest that the multimeric particles identified in the PB patterns of the M_2 receptor were not a product of disulfide-mediated aggregation or clusters of protomers within the same diffraction-limited spot; rather, they were extracted, purified, and immobilized as non-covalent complexes.

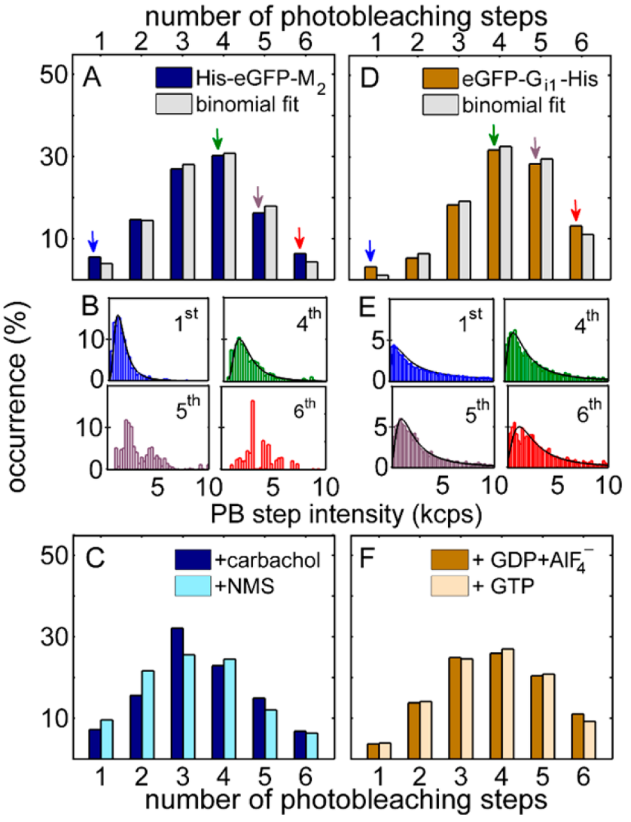

Figure 4. Photobleaching of purified M_2 receptor and G_{i1}. The distribution of the number of photobleaching steps is shown for immobilized particles of the receptor (His_6-eGFP-M_2) (A, C) and holo-G_{i1} (eGFP-$G\alpha_{i1}\beta_1\gamma_2$-$His_6$) (D, F), either alone (A, blue; D, brown) or in the presence of ligands (C, 10 μM carbachol, dark blue; 10 μM NMS, light blue. F, 10 μM GDP plus 10 μM AlF_4^-, dark brown; 10 μM GTPγS, light brown). Each histogram was analyzed in terms of the binomial distribution (eq 7, Table S3), shown as gray bars in panels A (receptor) and D (G_{i1}). The arrows in panels A and D identify steps for which the distributions of intensities are shown in panels B (receptor) and E (G_{i1}), where the lines represent the best fits of the GEV distribution (eq 8, Table S3).

Table 1. Average Number of Photobleaching Steps (N_{avg}) Observed with the eGFP-Tagged M_2 Receptor Alone or Coupled to G_{i1} with and without Muscarinic Ligands[a]

sample	no ligand	+ NMS	+ carbachol
His_6-eGFP-M_2[b]	3.6 ± 0.1	3.27 ± 0.10	3.43 ± 0.10
eGFP-M_2-$G\alpha_{i1}\beta_1$-His_6-γ_2[c]	3.4 ± 0.2[b]	1.92 ± 0.04[d]	—

[a]The final concentration of each ligand was 10 μM, and all samples were measured in the presence of 10 mM DTT. Parametric errors are shown as ± SEM. [b]The average number of photobleaching steps was estimated by fitting the binomial distribution (eq 7, $n = 6$) to the distribution of the number of steps ($N_{avg} = np$). The fitted values of p are listed in Table S3. [c]Samples were purified, immobilized, and measured in the presence of 10 μM carbachol. [d]The average number of photobleaching steps was estimated by fitting the Poisson distribution (eq 9) to the distribution of the number of steps ($N_{avg} = \lambda$).

Photobleaching of G_{i1}. Holo-G proteins containing eGFP-$G\alpha_{i1}$ were purified and immobilized via a hexahistidyl tag at the N-terminus of $G\gamma_2$ (eGFP-$G\alpha_{i1}\beta_1$-His_6-γ_2) (Figure 3A), thereby ensuring that PB measurements were done on heterotrimers. DTT was present throughout at a concentration of 10 mM.

DOI: 10.1021/jacs.6b04032
J. Am. Chem. Soc. 2016, 138, 11583−11598

The intensity traces displayed up to six smPB steps, with 92% of the particles showing more than two steps (Figure 4D). The smPB histogram was described by the binomial distribution (eq 7) with n taken as 6, and the fitted value of p (69.4%) corresponds to an average of 4.2 PB steps per particle (N_{avg}) (Table S3). All six PB steps gave distributions of intensities (Figure 4E) that were skewed like those of multiplexed eGFP, although the average intensity was somewhat larger ($I_{avg} \approx$ 1900 cps) (Table S3). Each of the six steps therefore appears to represent a single eGFP fluorophore, in contrast to the anomalous patterns obtained for steps 5 and 6 in the case of the receptor (Figure 4B). The consistency among all six PB steps suggests that G_{i1} is a hexamer in the absence of the receptor.

The addition of GTPγS or the sequential addition of GDP and AlF_4^- caused a small leftward shift in the smPB distributions (cf. Figures 4D,F). The maximum number of PB steps remained unchanged at six. In terms of the binomial distribution (eq 7, $n = 6$), the value of N_{avg} decreased marginally from 4.2 in the absence of ligand to 3.8 with GTPγS or to 3.9 with GDP followed by AlF_4^- (Table 2). The intensity distributions for all six PB steps were similar to those in the absence of ligand. Because the level of occupancy by GTPγS was about 90% (log $K = -6.01$, Figure 1D, Table S1), the 5- and 6-step traces likely arose from fully occupied G_{i1} rather than from a subpopulation of vacant G proteins. Guanylyl nucleotides therefore do not appear to affect the oligomeric state of heterotrimeric G_{i1}.

Table 2. Average Number of Photobleaching Steps (N_{avg}) Observed with eGFP-G_{i1}, eGFP-G_{i1} Coupled to M_2 Receptor, and eGFP-M_2 Receptor Coupled to G_{i1} with and without Ligands to $G\alpha_{i1}$[a]

sample	no ligand	+ GDP + AlF_4^-	+ GTPγS
eGFP-$G\alpha_{i1}\beta_1$-His_6-γ_2[b]	4.2 ± 0.1	3.90 ± 0.15	3.81 ± 0.12
His_6-eGFP-M_2-$G\alpha_{i1}\beta_1\gamma_2$[b,d]	3.4 ± 0.2	3.33 ± 0.06	3.56 ± 0.10
M_2–eGFP-$G\alpha_{i1}\beta_1$-His_6-γ_2[d]	3.3 ± 0.2[b]	2.43 ± 0.10[c]	2.11 ± 0.30[c]
His_6-eGFP-$G\alpha_{i1}$[b]	—	3.77 ± 0.13	3.74 ± 0.13
His_6-eGFP-$G\alpha_{i1}$ + Mas7	3.5 ± 0.1[b]	—	1.85 ± 0.12[c]

[a]The final concentration of each ligand was 10 μM, and all samples were measured in the presence of 10 mM DTT. Parametric errors are shown as ± SEM. [b]The average number of photobleaching steps was estimated by fitting the binomial distribution (eq 7, $n = 6$) to the distribution of the number of steps ($N_{avg} = np$). The fitted values of p are listed in Table S3. [c]The average number of photobleaching steps was estimated by fitting the Poisson distribution (eq 9) to the distribution of the number of steps ($N_{avg} = \lambda$). [d]Samples were purified, immobilized, and measured in the presence of 10 μM carbachol.

*Sf*9 cells express substrates for pertussis toxin,[47] and in some cases their levels may be similar to those of exogenous $G\alpha_{i1}$. The specific binding of [^{35}S]GTPγS in extracts from uninfected *Sf*9 cells was 45–65% of that in extracts of cells expressing His_6-tagged $G\alpha_{i1}$, measured at radioligand concentrations of 1.0 and 0.1 μM and expressed relative to total protein. It nevertheless appears that few if any endogenous G proteins were incorporated into oligomers of eGFP-G_{i1}; as argued below, such an incorporation would affect the fitted probability of detecting a single fluorophore but not the PB-based estimate of oligomeric size.

The data illustrated in Figure 4D are in good agreement with the binomial theorem when $n = 6$ (eq 7), and the fit is compromised at higher or lower values of n (SI, Section S4, Table S5). In the case of an octamer ($n = 8$), for example, particles with seven PB steps are predicted in numbers that are above the threshold of detection but were not observed (Figure S6). Endogenous G proteins are a form of dark protomer, and their stochastic incorporation into a multimeric complex of defined size would reduce the number of eGFP-tagged protomers in a predictable manner; in an oligomer of size n, such a dilution would be accompanied by a countervailing increase in the probability of exciting and detecting a fluorophore (SI Section S4).

In the case of eGFP-G_{i1} and $n = 6$, the probability of detecting a fluorophore would increase from 0.7 in the absence of dark protomers to 0.78, 0.88, and 1.0 with dark protomers at mole fractions of 0.1, 0.2, and 0.3, respectively (Table S5). Fitted values of p were ∼0.8 or less for $eGFP_{x4}$ and ∼0.6 for oligomers of the M_2 receptor (Table S3), thus suggesting that the mole fraction of endogenous G proteins in oligomers of eGFP-G_{i1} cannot exceed 0.1–0.2. That limit would be lower if protomers of G_{i1} were favored over the endogenous G proteins of *Sf*9 cells during assembly of the oligomer. Such a preference is consistent with evidence that the G proteins of *Sf*9 cells do not couple to M_2 muscarinic receptors.[47] Finally, extracts of *Sf*9 cells were immunonegative when probed with antibodies to mammalian $G\alpha_{i1-3}$ or $G\alpha_o$[47] (see also Figure S1C).

Photobleaching of Coupled M_2 Receptor and Holo-G_{i1}. Three complexes were purified in which eGFP was fused to the N-terminus of the receptor or inserted in $G\alpha_{i1}$ (Figure 3A). Coupling of receptor and G protein was ensured by the inclusion of carbachol throughout the purification and subsequent smPB assays. The location of the hexahistidyl tag used for immobilization of the fluorophore-tagged complexes was varied in order to detect uncoupling of the G protein from the M_2 receptor and related effects on the oligomeric size of either. With His_6 at the N-terminus of $G\gamma_2$, eGFP was placed within $G\alpha_{i1}$ or at the N-terminus of the receptor. The His_6 tag and eGFP also were fused in series to the N-terminus of the receptor. Thus, the oligomeric size of the M_2 receptor was estimated in complexes immobilized via the receptor or via the G protein, and the oligomeric size of the G protein was estimated in a complex immobilized via the G protein. This approach confirmed the presence of both proteins during measurements.

eGFP-Tagged M_2 Receptor Bound to $G\alpha_{i1}\beta_1\gamma_2$. The PB properties of the eGFP-tagged receptor were the same irrespective of whether the complex was immobilized via the G protein (eGFP-M_2-$G\alpha_{i1}\beta_1$-His_6-γ_2, Figure 5A) or the receptor (His_6-eGFP-M_2-$G\alpha_{i1}\beta_1\gamma_2$, Figure 5C) (see also Movie S1A). In each case, the intensity–time traces from single particles displayed a maximum of six PB steps. The smPB histogram resembled that obtained with eGFP-tagged M_2 receptor in the absence of G protein (Figure 4A), and at least 73% of the traces displayed more than two PB steps (Table S3).

With the complex tethered via G_{i1} (i.e., eGFP-M_2-$G\alpha_{i1}\beta_1$-His_6-γ_2), analysis of the data in terms of eq 7 ($n = 6$) gave values for p and N_{avg} of 54.5% and 3.4 steps per particle, respectively (Figure 5A, Table S3). PB steps 1–4 gave distributions of intensities that resemble, in shape and average intensity (I_{avg} = 1370 cps), those obtained from multiplexed eGFP and indicative of single fluorophores (e.g., steps 1 and 4, Figure 5B). Steps 5 and 6 were anomalous (Figure 5B). The PB properties of eGFP-M_2-$G\alpha_{i1}\beta_1$-His_6-γ_2 therefore resemble those of the M_2 receptor alone (cf. Figure 4A,B), suggesting that the

DOI: 10.1021/jacs.6b04032
J. Am. Chem. Soc. 2016, 138, 11583–11598

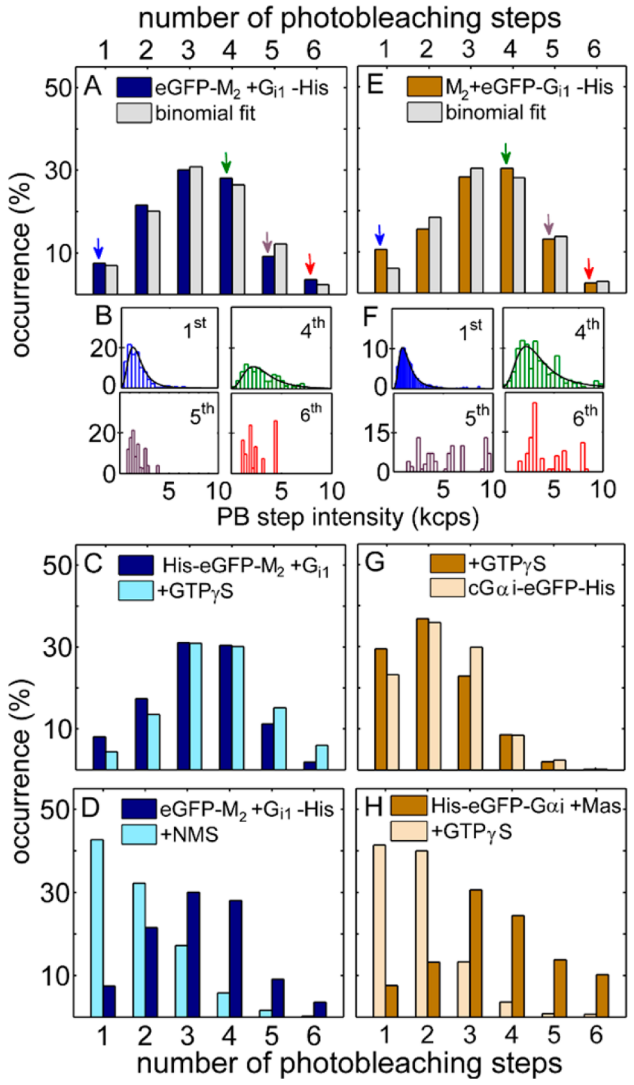

Figure 5. Photobleaching of G_{i1}-coupled eGFP-M_2 receptor, receptor-coupled eGFP-G_{i1}, and activated eGFP-$G\alpha_{i1}$. (A–D) A complex of the eGFP-tagged receptor plus holo-G_{i1} was purified and immobilized via a His_6 tag on $G\gamma_2$ (eGFP-M_2-$G\alpha_{i1}\beta_1$-His_6-γ_2) (A,D) or on the receptor-fused fluorophore (His_6-eGFP-M_2-$G\alpha_{i1}\beta_1\gamma_2$) (C). The distribution of the number of photobleaching steps is shown for the complex alone (A, C, and D, dark blue), in the presence of 10 μM GTPγS (C, light blue), and in the presence of 10 mM NMS (D, light blue). (E,G) A complex of the receptor plus holo-G_{i1} with eGFP inserted in $G\alpha_{i1}$ was purified and immobilized via His_6-$G\gamma_2$ (M_2-eGFP-$G\alpha_{i1}\beta_1$-His_6-γ_2). The distribution is shown for the complex alone (E, dark brown) and in the presence of 10 μM GTPγS (G, dark brown). Also in panel G is the distribution obtained for a purified, constitutively active mutant of $G\alpha_{i1}$ (Q204L) (His_6-eGFP-c$G\alpha_{i1}$, light brown). (H) The distribution obtained with purified His_6-eGFP-$G\alpha_{i1}$ was measured in the presence of 10 μM mastoparan (Mas) (dark brown) and in the presence of 10 μM mastoparan plus 10 μM GTPγS (light brown). (A,E) The gray bars show the best fit to the binomial distribution (eq 7, Table S3). The arrows in panels A and E identify steps for which the distributions of step intensities are shown in panels B and F, respectively, where the lines represent the best fits of the generalized extreme value distribution (eq 8, Table S3). All images were obtained in the presence of 10 mM DTT.

oligomeric status of the receptor is not affected by coupling of the G protein. Similar results were obtained with the complex tethered via the receptor (i.e., His_6-eGFP-M_2-$G\alpha_{i1}\beta_1\gamma_2$).

Neither GTPγS nor GDP plus AlF_4^- affected the distribution of PB steps (Figure 5C, Table 2) or the distributions of intensities obtained with His_6-eGFP-M_2-$G\alpha_{i1}\beta_1\gamma_2$. The oligomeric status of the M_2 receptor therefore was unchanged upon activation of the G protein by a guanylyl nucleotide plus carbachol, which was present throughout. In contrast, NMS shifted the PB histogram of eGFP-M_2-$G\alpha_{i1}\beta_1$-His_6-γ_2 markedly to the left (Figure 5D) and reduced the average number of PB steps (N_{avg}) from 3.4 (eq 7, $n = 6$) to 1.9 (eq 9) (Table 1). The ligand therefore appeared to reduce the number of protomers per particle when the receptor was immobilized via the G protein but not when immobilized alone (cf. Figure 4C, Table 1). The decrease in N_{avg} indicates that protomers of the receptor dissociate singly or in pairs rather than as the native oligomer. A concomitant decrease of 25–30% in the number of tethered spots suggests that all of the receptors eventually would be lost (Movie S2B). Owing to the likelihood that NMS creates a time-dependent mixture of oligomeric species, the data were analyzed as a Poisson distribution (eq 9).

M_2 Receptor Bound to eGFP-Tagged $G\alpha_{i1}\beta_1\gamma_2$. Intensity–time traces obtained with immobilized particles of M_2-eGFP-$G\alpha_{i1}\beta_2$-His_6-γ_2 displayed a maximum of six PB steps, and 74% of the traces showed more than two steps (Figure 5E). An analysis of the PB histogram in terms of the binomial distribution gave values for p and N_{avg} of 56% and 3.3 steps per particle, respectively (eq 7, $n = 6$) (Table S3). Steps 1–4 had intensity distributions that were consistent with eq 8 (I_{avg} = 1876 cps, Table S3) and resembled those of multiplexed eGFP, whereas steps 5 and 6 were anomalous (Figure 5F). The overall pattern therefore differs from that of G_{i1} without receptor, which gave GEV-like distributions for all six PB steps (Figure 4D). The distribution of PB steps also was left-shifted by the receptor, as indicated by the decrease in N_{avg} from 4.2 to 3.3 (Table S3) and in the complement of five- and six-step traces from 41% (Figure 4D) to only 16% (Figure 5E). The reduced occurrence of traces with five or six PB steps and the change in their intensity distributions suggest that G_{i1} is predominantly tetrameric when coupled to the M_2 receptor.

Activation of G_{i1} by GTPγS or by GDP plus AlF_4^- had no appreciable effect on the number of fluorescent spots but caused a marked leftward shift in the smPB histogram (Figure 5G). Five- and six-step traces were almost eliminated, and the fraction of one- and two-step traces increased from 26% to 66%. Such a shift implies a reduction in the number of G proteins per tethered particle, and the data were analyzed as a Poisson distribution (eq 9). The fitted values of λ (N_{avg}) are 2.11 and 2.43 for samples with GTPγS and GDP plus AlF_4^-, respectively.

Ligand-dependent changes in the PB histograms indicate that immobilized complexes of the receptor and G protein retain native functionality. The effects on G_{i1} appear to be a consequence of activation, inasmuch as they require the agonist-liganded receptor plus a guanylyl nucleotide. Fewer PB steps per particle suggest that the presumed tetramer undergoes fragmentation, leaving behind tethered monomers or dimers. Conversely, NMS causes a G_{i1}-dependent reduction in the oligomeric size of the receptor, although it is unclear whether the ligand acts by displacing carbachol or in its own right as an inverse agonist. Also unclear is whether the receptor departs alone or together with a complement of G proteins.

Photobleaching of Peptide-Activated and Constitutively Active eGFP-$G\alpha_{i1}$. The marked effect of nucleotide triphosphates on the PB histogram of receptor-coupled G

DOI: 10.1021/jacs.6b04032
J. Am. Chem. Soc. 2016, 138, 11583–11598

proteins suggests that G_{i1} binds as a tetramer to the agonist-occupied receptor and disaggregates into smaller oligomers or monomers upon activation by GTP (cf. Figures 4F and 5G). This possibility was tested by treating the fluorophore-tagged α_{i1}-subunit (i.e., His_6-eGFP-Ga_{i1}) with a 100-fold molar excess of mastoparan (Mas7), a peptide known to mimic the agonist-liganded receptor as an activator of Gα_{i1}.[48] The distribution of PB steps from Gα_{i1} plus mastoparan shows a maximum of six steps (Figure 5H, Movie S3A) and gave an average of 3.5 PB steps per particle ($N_{avg} = np$, eq 7, $n = 6$) (Table 2). GTPγS shifted the distribution leftward (Figure 5H, Movie S3B) and reduced the value of N_{avg} to 1.85 steps per particle (λ, eq 9) (Table 2). Both the distribution of PB steps and the effect of GTPγS resemble the results obtained with G_{i1} plus agonist-liganded receptor (Figures 5E,G). Dual activation of G_{i1} by the receptor and a guanylyl nucleotide therefore appears to reduce the oligomeric size of the G protein. The magnitude of the effect of GTPγS was somewhat greater with Gα_{i1} and mastoparan (Figure 5H) than with G_{i1} and agonist-liganded receptor (Figure 5G), as illustrated by the decrease in N_{avg} from 3.5 to 1.9 with the former and from 3.3 to 2.1 with the latter (Table 2).

To test further the possibility that oligomers of G_{i1} fragment upon activation, we measured a constitutively active α_{i1}-subunit obtained by substituting leucine for glutamine at position 204 (i.e., His_6-eGFP-cGα_{i1}).[49] At an excitation intensity of 155 W/cm^2, immobilized particles of purified His_6-eGFP-cGα_{i1} showed up to six PB steps, with 89% of the particles showing one to three steps and 59% showing one or two steps (Figure 5G). The distributions of intensities from steps 1−3 resembled those obtained with multiplexed eGFP (Figure S4D). At a lower excitation intensity of 60 W/cm^2, 82% of the particles showed mostly one or two PB steps; at a maximum intensity of 260 W/cm^2, however, the distribution was essentially the same as that at 155 W/cm^2 (Figure S5). A fit of the Poisson distribution (eq 9) to the data shown in Figure 5G gave a value for N_{avg} of ∼2.3 steps. The results indicate that larger oligomers ($n > 3$) are essentially absent from the sample.

Packing of Tetrameric M_2 Receptors and G Proteins. Data from FRET and smPB point to a complex of four receptors and four heterotrimeric G proteins. To demonstrate that such an arrangement is spatially feasible, a molecular model of the complex was simulated using molecular dynamics. The fundamental unit of packing was a complex of the M_2 receptor and G$\alpha_{i1}\beta_1\gamma_2$, which was computed by superimposing those elements on the corresponding proteins within the crystal structure of the complex formed by the β_2 adrenergic receptor and G_s (β_2AR-G_s) (PDB ID: 3SN6).[36] A comparison of Gα_{i1} and Gα_s performed in Clustal Omega indicated that the two α-subunits are similar in sequence and secondary structure. In the case of β_2AR-G_s, however, the Ras and helical domains of nucleotide-free Gα_s lie farther apart than do those domains in the nucleotide-bound structure of Gα_{i1} (1GIA). To accommodate this difference, the two α-subunits first were aligned by superimposing the region between Met[198] and the C-terminus of Gα_{i1} on the corresponding region of Gα_s. The M_2 receptor then was superimposed on the β_2 receptor while maintaining G$\beta_1\gamma_2$ in the position held by the $\beta\gamma$-heterodimer in the crystal structure of β_2AR-G_S (3SN6) (Figure 6A).

Complexes of the M_2 receptor and eGFP-G$\alpha_{i1}\beta_1\gamma_2$ were packed together to identify arrangements that can accommodate four heterotrimeric G proteins. Only one such arrangement maintained the interface between each receptor and its corresponding Gα_{i1}-subunit while avoiding overlap of neighboring G$\beta_1\gamma_2$ or eGFP (Figure 6). In that complex, adjacent receptors form an interface between transmembrane helices 4 and 5 (Figure 6A); at each interface, apolar amino acid side chains protrude toward the neighboring protein and foster hydrophobic interactions between the two helices. Adjacent G proteins form an interface between Glu[64] and Lys[68] within the helical domain of one α_{i1}-subunit and two regions of another: namely, the distal portion of helix αE near the guanine nucleotide-binding region and, in particular, the disordered loop between helices αE and αF (Q164−T170) (Figure 6B). In the resulting hetero-octamer of receptors and G proteins (Figure 6C, Movie S4), each protomer of receptor communicates directly with its coupled G protein and may communicate indirectly with the G protein coupled to a neighboring protomer.

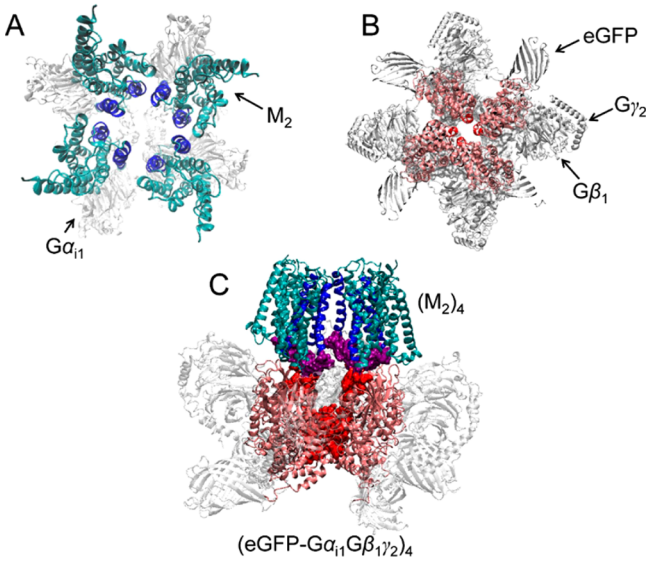

Figure 6. Proposed packing of the M_2 Receptor and eGFP-G$\alpha_{i1}\beta_1\gamma_2$ in a hetero-octamer comprising four copies of each. (A) Extracellular view of the tetramer of M_2 receptors. Transmembrane domains 4 and 5 are shown in dark blue and form a recurrent interface of oligomerization between adjacent protomers. Transmembrane domains 1−3 are shown in aqua. Gα_{i1} is shown in gray, and G$\beta_1\gamma_2$ and eGFP have been omitted for clarity. (B) Intracellular view of the tetramer of eGFP-G_{i1} (peach). The interface of oligomerization is shown in dark red. Gβ_1, Gγ_2, and eGFP are shown in gray, and the receptor is represented as a gray surface. (C) Side view of the hetero-octamer comprising four heterodimers of the receptor and eGFP-G_{i1} [i.e., (M_2-eGFP-G$\alpha_{i1}\beta_1\gamma_2$)$_4$]. Different regions are color-coded as in panels A and B. The region of the receptor making contact with Gα_{i1} is shown in purple.

Mastoparan mimicked the ability of the agonist-liganded receptor to cause an apparent disaggregation of holo-G proteins in the presence of GTPγS (cf. Figure 5G,H). The conformational basis of that change was explored in atomic-level simulations, which indicated that mastoparan adopts an α-helical conformation resembling a helix within the third intracellular loop of the M_2 receptor (Figure S5B). That arrangement places three lysine side-chains on the same side of the helix, where they may interact with the membrane. Simulations into the effect of mastoparan on the conformation of the α_{i1}-subunit were based on a crystal structure of Gα_{i1} occupied by GTPγS and Mg^{2+} (1GIA).[50] An initial calculation in ZDock was used to place mastoparan in two possible

DOI: 10.1021/jacs.6b04032
J. Am. Chem. Soc. 2016, 138, 11583−11598

locations near the α5 helix of $G\alpha_{i1}$, which is within the receptor-binding region. Over a short production period of 5 ns, both arrangements converged to a single position that served as the starting point for subsequent calculations (Figure S5).

In simulations on the longer time-scale of 30 ns, mastoparan had no large conformational effect on $G\alpha_{i1}$ under any condition. The α-helical and Ras domains remained closely associated throughout the process, in contrast to the spontaneous separation reported previously in the case of G_s.[12] Over the period of the simulation, however, those regions of $G\alpha_{i1}$ that form the interfaces of oligomerization in the model described above (Figure 6B) were the most dynamic, as indicated by fluctuations in the root-mean-square deviation of the backbone (Figure S5B). In particular, movement was observed in the loop between helices αE and αF (Q164−T170) and in part of the helical domain (E64−Q68) (Figure S5B−F). By disrupting the interface, conformational changes in those regions may lead to a disaggregation of the tetramer following activation of the G protein by the combination of GTP and either mastoparan or an agonist-liganded receptor.

DISCUSSION

G protein-coupled receptors are known to form oligomers in live cells and other preparations,[17,20,51] and those oligomers have been studied at some length for their prevalence, stability, and biological role.[52] In contrast, oligomers of G proteins have received relatively little attention. Aggregates of G_s, G_i, G_o, and G_q were detected early on in detergent-solubilized extracts from rat brain, and their disaggregation was implicated in signaling.[53] Also, the allosteric interaction between agonists acting at the receptor and guanylyl nucleotides acting at the G protein has prompted the suggestion that oligomers of GPCRs imply oligomers of G proteins.[54] Coupling of two such oligomeric partners would be expected to yield a ligand-sensitive complex of receptors and G proteins such as the heteromeric octamer described here.

Oligomers of the M_2 receptor alone have been confirmed by smPB, in which immobilized particles of the purified eGFP-tagged receptor displayed up to six PB steps. The distributions of intensities from only four of those steps resembled the distributions from single fluorophores in multiplexed controls, suggesting that the receptor was purified as a tetramer. The oligomeric state of the receptor was essentially unaffected by muscarinic ligands, in that the average number of PB steps was virtually identical in the absence of ligand and in the presence of NMS or carbachol (Table 1). These observations agree with previous results based on mechanistic modeling,[8,13] electrophoretic mobility after cross-linking,[13] and FRET between fluorophore-tagged protomers in live cells,[20] all of which have suggested that the M_2 muscarinic receptor exists wholly or in part as a tetramer.

Several lines of evidence indicate that $G\alpha_{i1}$ and holo-G_{i1} also exist as oligomers, both in live CHO cells and after purification from *Sf*9 membranes. Multimeric forms of G_{i1} in CHO cells were detected by dcFCS and, independently, by FRET between α-subunits tagged with eGFP or mCherry. The degree of cross-correlation between the two spectral channels in dcFCS indicated that at least 50% of the diffusing particles contained both fluorophores, which is an unambiguous signature of proteins that co-diffuse as oligomers (Figure 2A). The apparent FRET efficiency measured with holo-G_{i1} increased with the ratio of acceptor to donor in a saturable manner, leveling off at 50−75% (Figure 2C). That dependence was invariant over a 64-fold range of total expressed eGFP- and mCherry-tagged $G\alpha_{i1}$; also, the levels of expression at the lower end of that range were similar to those in cells that displayed a significant degree of cross-correlation in dcFCS. Model-based estimates of the pairwise FRET efficiency between a single donor and a single acceptor suggest that oligomers of G_{i1} detected by FRET comprise at least four heterotrimeric G proteins. The possibility that the interactions detected by dcFCS and FRET contain a stochastic component was ruled out in parallel studies with a non-interacting control (Figures 2A,C,D).

In agreement with the FRET-based estimate of oligomeric size in CHO cells, the results of smPB point to hexamers of eGFP-tagged $G\alpha_{i1}$ purified from *Sf*9 cells with or without $G\beta_1\gamma_2$. The average number of PB steps per particle was the same for $G\alpha_{i1}$ (N_{avg} = 3.8 steps) and holo-G_{i1} (N_{avg} = 3.9 steps), suggesting that the oligomer of holo-G_{i1} is stabilized primarily by interactions between the α-subunits (Table 2). The reducing environment experienced by G proteins in live cells[55] was maintained during extraction and purification by the inclusion of DTT at a concentration of 10 mM. Reactive cysteine residues therefore are unlikely to account for the stability of oligomers identified by stepwise PB.

A complex of the M_2 receptor and G_{i1} was purified in three forms that differed in the locations of eGFP and the hexahistidyl tag. The fluorophore was located on $G\alpha_{i1}$ or the receptor, and His_6 was located on the receptor or $G\gamma_2$ (Figure 3A). Each form was characterized by single-particle PB, and the distributions of PB steps indicated that the composition of the complex was the same irrespective of the locations of the tags. [^{35}S]GTPγS bound to the purified complex with two affinities, each of which was appreciably higher than the single affinity observed with $G\alpha_{i1}$ or holo-G_{i1} alone (Figure 1E, Table S1). Each preparation therefore appeared to be homogeneous and, in particular, to be devoid of unbound G proteins; that is, complexes purified via His_6-tagged $G\gamma_2$ had their full complement of receptors, and those purified via His_6-tagged M_2 receptor had their full complement of G proteins.

The appearance of heterogeneity in the binding of [^{35}S]GTPγS, indicates that oligomers of receptor-bound G proteins can adopt multiple conformations that are essentially unpopulated with oligomers of the G protein alone. Such effects may arise through cooperativity in the binding of the nucleotide,[42,54] and a similar binding profile has been reported previously for a complex of M_2 receptors and G proteins purified from porcine sarcolemma.[42] The similarity suggests that the purified complexes detected by smPB are biologically relevant.

Coupling of the M_2 receptor and G_{i1} resulted in a supramolecular complex of four receptors and four G proteins, as indicated in each case by the predominance of particles with 1−4 PB steps. A 1:1 stoichiometry is supported by the average number of PB steps per particle, which was the same for the receptor (N_{avg} = 3.4 steps) and for G_{i1} (N_{avg} = 3.3 steps). In contrast to free G_{i1}, which was unaffected by guanylyl nucleotides, receptor-coupled G_{i1} was tetrameric in the absence of nucleotide or in the presence of GDP but appeared to be predominantly dimeric and monomeric in the presence of GTPγS or GDP plus AlF_4^- (Table 2); the agonist carbachol was present throughout. Simultaneous activation of the M_2 receptor and G_{i1} therefore reduced the oligomeric size of the latter. This was confirmed by replacing the receptor with the peptide mimic mastoparan, which competes with the receptor

DOI: 10.1021/jacs.6b04032
J. Am. Chem. Soc. 2016, 138, 11583−11598

for the G protein[56] and can activate $G\alpha_{i1}$.[48] Mastoparan has been shown by NMR to mimic the third intracellular loop of the M_2 receptor,[48] and molecular dynamics simulations have shown that it binds to α-helix 5 of $G\alpha_{i1}$ (Figure S5B). As predicted, the size of immobilized G_{i1} in PB assays was reduced when mastoparan was added together with GTPγS (N_{avg} = 1.85) but not when it was added alone (N_{avg} = 3.54) (Table 2).

The feasibility of packing four receptors and four holo-G proteins in a supramolecular complex was demonstrated in molecular dynamics simulations (Figure 6, Movie S4). The structure was computed from the starting point of a heterodimer (i.e., RG), but the different multimeric components all can be purified or reconstituted independently (i.e., R_4, G_4, and RG). Assembly of the complex within the cell therefore could be envisaged as the formation of a dimer of homotetramers (i.e., R_4G_4) or a tetramer of heterodimers (i.e., $(RG)_4$). Either way, the interface of oligomerization between contiguous receptors is formed between transmembrane helices 4 and 5 (Figure 6A). The same interface has been implicated in the oligomerization of other GPCRs of Family 1A: by chemical cross-linking in the case of the D_2 dopamine[57] and M_3 muscarinic receptors,[58] and by cross-linking,[59] X-ray crystallography,[60] and peptide disruption[61] in the case of rhodopsin.

The interface of oligomerization between contiguous G proteins is formed by the disordered loop between helices αE and αF (Q164−T170) of one α_{i1}-subunit and residues E64−K68 within the helical domain of another (Figure 6B). That region is comparatively dynamic (Figure 6B, Figure S5), and the flexibility may facilitate the disassembly observed by PB. Disassembly may expose interfaces that are inaccessible within the tetramer, making them available for interactions with other effectors. Because guanylyl nucleotides had no effect on the distributions of PB steps obtained with $G\alpha_{i1}$ or holo-G_{i1} alone, any such conformational rearrangement appears to require the presence of the receptor.

Tagged $G\alpha_{i1}$-subunits were used throughout these studies, and their functionality was unaffected by insertions after position 91 or by purification. Purified His_6-tagged $G\alpha_{i1}$ underwent characteristic ligand-dependent conformational changes that were detected in the fluorescence of tryptophan 211 (Figure S1E), and the affinity of [^{35}S]GTPγS for purified eGFP- and mCherry-tagged $G\alpha_{i1}$ was similar to that reported previously for purified G proteins or Gα-subunits.[62] Fluorophore-tagged $G\alpha_{i1}$ formed a heterotrimer with $G\beta_1\gamma_2$ and coupled to the M_2 receptor. The presence of heterotrimeric G_{i1} was indicated by the co-migration of mCh-$G\alpha_{i1}$ and eGFP-$G\beta_1$ in the membrane of CHO cells (Figure 1D) and by the stepwise PB of purified eGFP-$G\alpha_{i1}\beta_1\gamma_2$ immobilized via the γ-subunit (Figure 4D). Based on the time-scale of the smPB experiments, such complexes were stable for at least 2−3 h. Coupling of $G\alpha_{i1}$ to the M_2 receptor was evident from GDP- and GTP-sensitive FRET between eGFP-$G\alpha_{i1}$ and M_2-mCh (Figure 1C), and dissociation of $G\alpha_{i1}$ from the activated complex was indicated by a decrease in the average number of PB steps in the presence of carbachol and GTPγS (Figure 5G). These observations indicate that the insertion of a 27-kDa fluorophore had no discernible effect on the functioning of $G\alpha_{i1}$. Models simulated by molecular dynamics suggest that the fluorophore projects away from $G\alpha_{i1}$ in a manner that avoids steric conflicts with either the receptor or the G$\beta\gamma$ heterodimer (Figure 6, Movie S4).

Whereas smPB has identified a complex of four M_2 receptors and four G proteins, a different composition has been found previously for other GPCRs. Complexes containing two receptors and one G protein have been reported for rhodopsin[63] and the leukotriene B_4 receptor.[64] At the level of the G protein, one α-subunit has been shown to bind two $\beta\gamma$-heterodimers.[65] Such differences may be due to different receptors, but they also may arise from procedural differences in the preparation of the sample. All of the complexes characterized by smPB were purified as such from *Sf*9 cells by means of hexahistidyl tags and chelating chromatography. Coupling of the receptor and G_{i1} was maintained by inclusion of the agonist carbachol and the exclusion of GDP. In contrast, the preparations described above were reconstituted from purified GPCRs and G proteins or subunits thereof. Oligomers of GPCRs can disaggregate during purification to emerge as monomers,[17] and the native state may not be recovered upon reconstitution.

In single-particle studies of fluorescent proteins, oligomeric size is inferred from the number of PB steps and their intensities. To calibrate this relationship, we examined the PB patterns of purified controls comprising single and multiplexed units of eGFP (Figure S2A). Each control was purified from *E. coli* and immobilized in the manner of the M_2 receptor and G_{i1}. The complement of fluorophores was confirmed by its electrophoretic mobility (Figure S2B). Almost all spots of unitary eGFP showed a single PB step (~97%, Figure 3B), and the number of steps observed with duplex and quadruplex eGFP never exceeded two or four, respectively (Figure 3C,D). It follows that the intensity within a diffraction-limited spot derived from one and only one molecule of the control or, by extension, from one complex of eGFP-tagged receptor or G_{i1}.

When single particles of labeled GPCRs were tracked previously in live cells,[23,66] the fluorescence intensities gave skewed Gaussian-like distributions similar to those described here (e.g., Figures 3B and 4B,E). It was assumed in the analyses of those distributions that the signal detected from a single fluorophore under a TIRF microscope is normally distributed, leading to the conclusion that the receptors were predominantly monomeric with a minor contingent of dimers. A different picture emerges from our measurements of single and multiplexed eGFP, which show that a skewed distribution of intensities is characteristic of a single fluorophore (Figure 3B). Such asymmetry could arise from an inhomogeneous illumination field in the objective-based TIRF microscope and from the readout noise associated with weak signals in the electron-multiplying CCD camera.

The distribution of the number PB steps generated by single-particle PB typically is attributed to a mixture of species that differ in oligomeric size or, more specifically, in the number of fluorophores. An alternative explanation emerges from the experiments with purified multiplexed controls, where the distribution of intensities obtained with $eGFP_{x4}$ was shifted to the right or the left by changes in the laser excitation intensity. Such behavior indicates that the shape of the distribution is not a manifestation of heterogeneity within the sample; rather, it is a measure of the number of fluorophores that are simultaneously excited and detected within the multiplex or oligomer. We therefore suggest that the distribution of the number of PB steps is in fact a binomial distribution defined by the total number of fluorophores (i.e., tagged monomers) within the oligomer and the independent probability of exciting and detecting a single fluorophore.

DOI: 10.1021/jacs.6b04032
J. Am. Chem. Soc. 2016, 138, 11583−11598

CONCLUSIONS

We have determined the supramolecular organization of the M_2 muscarinic receptor and holo-G_{i1} by single-molecule photobleaching of eGFP fused to immobilized receptors or $G\alpha_{i1}$-subunits. The receptor and the G protein were purified from *Sf*9 cells both independently and together, and the oligomeric status of each was inferred from statistical analyses of the number of photobleaching steps. The M_2 receptor alone was purified as a tetramer, and the oligomeric state was unaffected by muscarinic ligands; G_{i1} alone was purified as a hexamer that was unaffected by GTPγS. Oligomers of G_{i1} larger than dimers were identified in live CHO cells by dcFCS and FRET, indicating that such structures are biologically relevant. Single-molecule photobleaching of a purified complex of the agonist-bound receptor and nucleotide-free G protein identified a hetero-octamer that comprised a tetramer of the M_2 receptor and a tetramer of heterotrimeric G_{i1}. The structural feasibility of such a complex was demonstrated by molecular dynamics simulations. Activation of the complex by GTPγS plus the agonist carbachol was accompanied by a reduction in the oligomeric size of G_{i1} from a tetramer to dimers and perhaps to monomers, while the receptor remained a tetramer. The basal and active states of G_{i1} therefore appear to differ in oligomeric size.

These results provide direct evidence for oligomers that have been inferred previously from mechanistic analyses of the binding properties of the M_2 muscarinic receptor and its attendant G proteins.[8,9,54] The symmetry of the proposed complex provides a structural basis for the reciprocal effects of guanylyl nucleotides on the binding of agonists to the receptor and of agonists on the binding of GDP to the G protein. Those effects are a manifestation of efficacy and signaling at the level of the receptor and G protein, and they have been attributed to co-operative interactions within a heteromeric array such as that identified here.[13,15,35] Disassembly of the oligomeric G protein within such a hetero-oligomeric signaling complex may allow the receptor to engage other effectors, leading to activation of different pathways and multiple signaling outcomes.

EXPERIMENTAL SECTION

Fluorescence Correlation Spectroscopy. FCS was performed on a Nikon Eclipse TI confocal microscope using a Plan-Apochromat water-immersion objective (40×, 1.2 NA). CHO cells were grown in glass-bottom culture dishes (MatTek. P35G-1.0-14-C) and transfected at 60% confluency. Measurements generally were performed on the top membrane of live cells 36−48 h after transfection using simultaneous excitation with blue (488 nm) and green (561 nm) lasers. The excitation power at the exit of the objective lens generally was set to about 0.5 μW for each laser.

Autocorrelation curves obtained for eGFP ($G_g(\tau)$) and mCherry ($G_r(\tau)$) were fit by a two-dimensional anomalous diffusion model that also includes triplet states for each fluorophore:[67]

$$G_i(\tau) = \frac{1}{N_i}\left(1 + \frac{\tau}{\tau_{D,i}}\right)^{-\alpha}\left(1 + \frac{f_{T,i}}{1 - f_{T,i}}e^{-t/\tau_{T,i}}\right) \quad (1)$$

The parameter N_i in eq 1 is the average number of particles in the detection volume, and τ_D is their average diffusion time; τ_T and f_T are the lifetime of the triplet state and the corresponding fraction of fluorophores, respectively. Effects of molecular crowding are quantified by deviations of the exponent α from 1. Values of α between 0.7 and 0.9 have been reported for proteins that undergo anomalous diffusion in the cell membrane.[68]

Cross-correlation curves were fit by eq 2,[69] in which N_x is the average number of co-diffusing species in the common detection area; N_g and N_r are the average numbers of the individual species (green and red) and were estimated from the autocorrelation data in terms of eq 1.

$$G_x(\tau) = \frac{N_x}{N_g N_r}\left(1 + \frac{\tau}{\tau_{D,x}}\right)^{-\alpha} \quad (2)$$

The values of N were used to calculate the fraction of each fluorophore that co-diffuses with the other (i.e., eGFP, $f_g = N_x/N_r$; mCherry, $f_r = N_x/N_g$).

Förster Resonance Energy Transfer. Details regarding the measurement of FRET are described in the SI, Section S2. Briefly, confocal fluorescence imaging was performed on a Zeiss microscope (LSM710) equipped with a Plan-Apochromat oil-immersion objective (63×, 1.4 NA). The cells were illuminated at 488 nm and an average intensity of ~500 W/cm^2. A typical imaging area of 135 μm × 135 μm was scanned between 495 and 640 nm using a detection window with a spectral width of 5 nm, and the resulting stack of 30 images was used to construct the fluorescence emission spectrum for a defined region of the cell membrane. The spectrum was unmixed by linear regression according to eq 3 to obtain the individual contributions of donor (k_D) and acceptor (k_A). Those values then were used to estimate the apparent FRET efficiency (E_{app}) according to eq 4,[70] taking into account the quantum yields of the fluorophores ($\Phi_{D,A}$) and the corresponding fractions of the spectral integrals measured in our experiments ($W_{D,A}$).

$$F(\lambda) = k_D F_D(\lambda) + k_A F_A(\lambda) \quad (3)$$

$$E_{app} = \left(1 + \frac{k_D}{k_A}\frac{\Phi_A}{\Phi_D}\frac{W_A}{W_D}\right)^{-1} \quad (4)$$

The dependence of the measured FRET efficiency on the ratio of acceptor to donor ([A]/[D]) was fitted by eq 5[40] to obtain the pairwise efficiency (E_p) for FRET between a single donor and a single acceptor in an oligomer of specified size (i.e., n = 2, 3, 4, 6, and 8).

$$E_{app} = \frac{1}{n}\sum_{k=1}^{n-1}\frac{k(n-k)E_p}{1 + (n-k-1)E_p}\binom{n}{k}P_D^{k-1}P_A^{n-k} \quad (5)$$

The ratio of acceptor to donor enters into the model as the mole fraction of each (i.e., P_A = [A]/([A] + [D]) and P_D = [D]/([A] + [D]), and k is the number of donors within the oligomer. The values of [A] and [D] for the region of interest were calculated according to the Beer−Lambert law (SI, eqs S2 and S3), and [D] was corrected for the loss of intensity through energy transfer. More details are described in the SI, Section S2. Photobleaching was minimal over the period of the measurements, as indicated by the values of [D] before and after imaging.

Preparation and Functionality of Receptor and G protein. Full details regarding the cloning, expression, and purification of various tagged forms of the M_2 receptor, holo-G_{i1}, $G\alpha_{i1}$, and complexes of the receptor and G_{i1} are described in the SI, Section S1. Briefly, the receptor and subunits of G_{i1} were expressed or co-expressed in CHO cells or baculovirus-infected *Sf*9 cells. eGFP and multiplexed eGFP to be used as controls were expressed in *E. coli*. All protein samples were purified by gravity-flow chromatography using Ni^{2+}-NTA agarose (Qiagen) (Figure S1).

In the case of samples containing $G\alpha_{i1}$, the functionality of the purified protein was assessed by monitoring the fluorescence of tryptophan 211 and in binding assays with the radiolabeled nucleotide [^{35}S]GTPγS (Figure S1). The binding curves were analyzed in terms of eq 6 to obtain estimates of the Hill coefficient ($n_{H,j}$) and the corresponding affinity (K_j) for each component j in a mixture of m components.

DOI: 10.1021/jacs.6b04032
J. Am. Chem. Soc. 2016, 138, 11583−11598

$$B_{obs}([P]_t) = B_{max} \sum_{j=1}^{m} \frac{F_j([P]_t - B_{sp})^{n_{H,j}}}{K_j^{n_{H,j}} + ([P]_t - B_{sp})^{n_{H,j}}} + NS([P]_t - B_{sp}) \quad (6)$$

More details regarding the binding of radioligands and related analyses are given in the SI, Section S1.

Immobilization of Single Particles. Glass coverslips and coverslides used in the construction of flow-chambers were cleaned and treated according to a procedure adapted from Jain et al.[71] as described in the SI, Section S3. Briefly, the surfaces were functionalized using 3-aminopropyl-triethoxysilane (APTES) and passivated with a mixture of 95% polyethylene glycol (mPEG SVA, MW 5000, Laysan Bio) and ~5% PEG-biotin (Biotin-PEG-SVA, MW 5000, Laysan Bio). Streptavidin was layered onto the biotinylated surface and followed in turn by the biotinylated-anti-His_6 antibody, which effected the immobilization of fluorescently labeled His_6-tagged proteins. To probe for ligand-induced changes, complexes that included a His_6-tagged protein were diluted in an appropriate buffer containing the ligand of interest and allowed to incubate for an additional 30 min at 20 °C prior to immobilization.

TIRF Microscopy. Fluorescence images were acquired on a locally constructed, objective-based TIRF microscope.[72] Solutions of purified $eGFP_{xj}$, M_2 receptor, holo-G_{i1}, or the receptor-G protein complex were added to the sample-chamber at a concentration of 1−10 nM, and the average density of immobilized particles was 0.01−0.10 μm^{-2}. The M_2 receptor was purified in the absence of a reducing agent. G_{i1} and complexes of the receptor plus G_{i1} were purified in the presence of β-mercaptoethanol (10 mM). All samples were imaged in the presence of DTT (10 mM) unless stated otherwise.

Samples were excited using a 473 nm laser (Cobolt Blue), and the emission from eGFP was captured by an Andor EMCCD camera (DU-897BV) after passage through a filter that selects for wavelengths of 500−525 nm. The area of illumination was typically 50 μm × 50 μm, and a movie consisting of 500 frames was acquired at a dwell-time of 30 ms per frame (i.e., 15 s) (Movies S1-S3). Several areas of the sample chamber were imaged in one experiment, and the experiments were repeated several times on the same type of sample. In samples without ligand, a total of 1500−2500 single-particle traces were analyzed per sample. In ligand-containing samples, a total of 500−1500 single-particle traces were analyzed. Those samples in which the ligand had little or no effect were at the lower end of this range (i.e., ~500 traces), and those affected by the ligand were at the higher end (i.e., 1000−1500 traces).

Analysis of Single-Molecule Photobleaching. Details regarding the processing of images, the extraction of fluorescence intensity−time traces from single particles, and the analyses of those traces are presented in the SI, Section S4. In short, a custom-written program in Matlab (MathWorks) was used to identify single particles (spots) in a sequence of frames, remove overlapping spots, and filter out the spikes and blinks that occur in such traces. Downward change-points were identified by a second program based on the principles laid out by Watkins and Yang[73] (Figure S3G). Steps with a drop in intensity of less than 500 cps were not counted, based on the PB characteristics of the monomeric eGFP control under the same conditions (Figure 3B). The results from all traces in a sample were assembled as histograms depicting the numbers of PB steps per particle, the drop in intensity per step, and the initial intensity.

Successive PB steps within the same intensity trace were indexed from the bottom up; that is, the last step before complete PB was termed step number 1, the previous step was number 2, and so on (Figure S3G). The distribution of the number of PB steps identified per particle (k) was fitted by the binomial distribution:

$$f(k; n, p) = \frac{n!}{k!(n-k)!} p^k (1-p)^{n-k} \quad (7)$$

The underlying assumption is that each particle (oligomer) comprises a discrete number of n independent subunits (protomers), each of which has one eGFP fluorophore with an equal probability (p) of excitation and detection. The reported values for n and p were obtained by fitting the data using a maximum-likelihood estimator (MLE) with a confidence interval of 95%.

The distribution of intensities associated with each indexed PB step was fitted by the generalized extreme value (GEV) distribution (SI, Section S4):

$$f(I; \mu, \sigma, \xi) = \frac{1}{\sigma}\left(1 + \xi\frac{I-\mu}{\sigma}\right)^{(-1/\xi)-1} \exp\left[-\left(1 + \xi\frac{I-\mu}{\sigma}\right)^{-1/\xi}\right] \quad (8)$$

Under certain conditions, treatment with a ligand to the M_2 receptor or G_{i1} appeared to reduce the size of the oligomer. In such cases, the histograms of the number of PB steps were fitted by a Poisson distribution in which λ is the expectation value (average):

$$f(k; \lambda) = \frac{\lambda^k e^{-\lambda}}{k!} \quad (9)$$

Molecular Modeling. Models of the M_2 receptor tagged with mCherry and of $G\alpha_{i1}$ tagged with eGFP were generated using MOE2013.0802 and refined by atomistic molecular dynamics simulations in Gromacs 4.6.5.[74,75] A model of the complex comprising the M_2 receptor and G_{i1} tagged in the α-subunit with eGFP was obtained by sequence alignment and structural superposition with the crystal structure of the complex formed by the β_2-adrenergic receptor and G_s (PDB ID: 3SN6). Atomistic molecular dynamics simulations of $G\alpha_{i1}$ (PDB ID: 1GIA) in explicit solvation were performed using the CHARMM27 force field in Gromacs 4.6.5. Simulations were carried out for $G\alpha_{i1}$ alone, complexed with GTP-Mg^{2+}, and complexed with GTP-Mg^{2+} and mastoparan. Conformational changes were tracked by fluctuations in the root-mean-square deviation of the peptide backbone.

■ ASSOCIATED CONTENT

Supporting Information

The Supporting Information is available free of charge on the ACS Publications website at DOI: 10.1021/jacs.6b04032.

Procedures and related data for the expression, purification, and characterization of receptor, G protein, and multiplexed eGFP (Section S1, Figure S1A−F, Figure S2, Table S1); FRET-based procedures for the detection and characterization of oligomers of G protein in CHO cells (Section S2, Figure S1G, Table S2); flow chamber, instrumentation, data analysis, and parametric values for smPB (Sections S3 and S4, Figures S3, S6, and S7, Tables S3−S5); smPB measurements of constitutively active $G_{\alpha i1}$ (Section S5, Figure S4); and molecular dynamics simulations (Section S6, Figure S5) (PDF)

Movie S1, single-molecule TIRF of purified complexes of the M_2 receptor and G_{i1} (MPG)

Movie S2, single-molecule TIRF of copurified M_2 receptor and G_{i1} in the presence of NMS (MPG)

Movie S3, single-molecule TIRF of purified $G\alpha_{i1}$ in the presence of mastoparan and GTPγS (MPG)

Movie S4, molecular dynamic simulation of a hetero-octamer of the M_2 receptor and holo-G_{i1} (MPG)

Captions to Movies S1−S4 (PDF)

■ AUTHOR INFORMATION

Corresponding Authors

*rvshiv@stanford.edu

*jwells@phm.utoronto.ca

*claudiu.gradinaru@utoronto.ca

DOI: 10.1021/jacs.6b04032
J. Am. Chem. Soc. 2016, 138, 11583−11598

Present Address

[▽]R.V.S.: Department of Molecular and Cellular Physiology, Stanford University School of Medicine, Stanford, CA 94305, USA

Author Contributions

[⊗]R.V.S., D.D.F., and H.J. made equal contributions to this work.

Notes

The authors declare no competing financial interest.

■ ACKNOWLEDGMENTS

We thank Dr. Donald F. Weaver of the Krembil Research Institute, University Health Network, for providing the facilities used for the molecular dynamics simulations. R.V.S and D.D.F. were supported by Ontario Graduate Scholarships (OGS). Y.L. and Z.Z. were supported by Training Grants from the Canadian Institutes of Health Research (CIHR). The work was supported by grants from the Heart and Stroke Foundation of Ontario (G140006078 to J.W.W.), the CIHR (MOP97978 to J.W.W.), and the Natural Sciences and Engineering Research Council of Canada (NSERC) (RGPIN 371705 to J.V.R., RGPIN 342295-12 to C.C.G).

■ REFERENCES

(1) Fredriksson, R.; Lagerstrom, M. C.; Lundin, L. G.; Schioth, H. B. *Mol. Pharmacol.* **2003**, *63*, 1256.
(2) Christopoulos, A.; Kenakin, T. *Pharmacol. Rev.* **2002**, *54*, 323.
(3) Maudsley, S.; Martin, B.; Luttrell, L. M. *J. Pharmacol. Exp. Ther.* **2005**, *314*, 485.
(4) Magalhaes, A. C.; Dunn, H.; Ferguson, S. S. G. *Br. J. Pharmacol.* **2012**, *165*, 1717.
(5) Overington, J. P.; Al-Lazikani, B.; Hopkins, A. L. *Nat. Rev. Drug Discovery* **2006**, *5*, 993.
(6) Kang, D. S.; Tian, X.; Benovic, J. L. *Methods Enzymol.* **2013**, *521*, 91.
(7) DeLean, A.; Stadel, J. M.; Lefkowitz, R. J. *J. Biol. Chem.* **1980**, *255*, 7108.
(8) Chidiac, P.; Green, M. A.; Pawagi, A. B.; Wells, J. W. *Biochemistry* **1997**, *36*, 7361.
(9) Green, M. A.; Chidiac, P.; Wells, J. W. *Biochemistry* **1997**, *36*, 7380.
(10) Hein, P.; Frank, M.; Hoffmann, C.; Lohse, M. J.; Bunemann, M. *EMBO J.* **2005**, *24*, 4106.
(11) Alexander, N. S.; Preininger, A. M.; Kaya, A. I.; Stein, R. A.; Hamm, H. E.; Meiler, J. *Nat. Struct. Mol. Biol.* **2014**, *21*, 56.
(12) Dror, R. O.; Mildorf, T. J.; Hilger, D.; Manglik, A.; Borhani, D. W.; Arlow, D. H.; Philippsen, A.; Villanueva, N.; Yang, Z.; Lerch, M. T.; Hubbell, W. L.; Kobilka, B. K.; Sunahara, R. K.; Shaw, D. E. *Science* **2015**, *348*, 1361.
(13) Ma, A. W.; Redka, D. S.; Pisterzi, L. F.; Angers, S.; Wells, J. W. *Biochemistry* **2007**, *46*, 7907.
(14) Kenakin, T. *Chem. Rev.* **2016**, DOI: 10.1021/acs.chemrev.5b00561.
(15) Redka, D. S.; Morizumi, T.; Elmslie, G.; Paranthaman, P.; Shivnaraine, R. V.; Ellis, J.; Ernst, O. P.; Wells, J. W. *J. Biol. Chem.* **2014**, *289*, 24347.
(16) Comps-Agrar, L.; Kniazeff, J.; Nørskov-Lauritsen, L.; Maurel, D.; Gassmann, M.; Gregor, N.; Prézeau, L.; Bettler, B.; Durroux, T.; Trinquet, E.; Pin, J. P. *EMBO J.* **2011**, *30*, 2336.
(17) Park, P. S.; Wells, J. W. *Biochemistry* **2003**, *42*, 12960.
(18) Hu, J.; Thor, D.; Zhou, Y.; Liu, T.; Wang, Y.; McMillin, S. M.; Mistry, R.; Challiss, R. A.; Costanzi, S.; Wess, J. *FASEB J.* **2012**, *26*, 604.
(19) McMillin, S. M.; Heusel, M.; Liu, T.; Costanzi, S.; Wess, J. *J. Biol. Chem.* **2011**, *286*, 28584.
(20) Pisterzi, L. F.; Jansma, D. B.; Georgiou, J.; Woodside, M. J.; Chou, J. T. C.; Angers, S.; Raicu, V.; Wells, J. W. *J. Biol. Chem.* **2010**, *285*, 16723.
(21) James, J. R.; Oliveira, M. I.; Carmo, A. M.; Iaboni, A.; Davis, S. J. *Nat. Methods* **2006**, *3*, 1001.
(22) Lan, T. H.; Liu, Q.; Li, C.; Wu, G.; Steyaert, J.; Lambert, N. A. *Sci. Rep.* **2015**, *5*, 10166.
(23) Hern, J. A.; Baig, A. H.; Mashanov, G. I.; Birdsall, B.; Corrie, J. E.; Lazareno, S.; Molloy, J. E.; Birdsall, N. J. *Proc. Natl. Acad. Sci. U. S. A.* **2010**, *107*, 2693.
(24) Kasai, R. S.; Suzuki, K. G.; Prossnitz, E. R.; Koyama-Honda, I.; Nakada, C.; Fujiwara, T. K.; Kusumi, A. *J. Cell Biol.* **2011**, *192*, 463.
(25) Herrick-Davis, K.; Grinde, E.; Mazurkiewicz, J. E. *Biochemistry* **2004**, *43*, 13963.
(26) Jain, A.; Liu, R.; Ramani, B.; Arauz, E.; Ishitsuka, Y.; Ragunathan, K.; Park, J.; Chen, J.; Xiang, Y. K.; Ha, T. *Nature* **2011**, *473*, 484.
(27) Ganguly, S.; Clayton, A. H. A.; Chattopadhyay, A. *Biophys. J.* **2011**, *100*, 361.
(28) Fung, J. J.; Deupi, X.; Pardo, L.; Yao, X. J.; Velez-Ruiz, G. A.; Devree, B. T.; Sunahara, R. K.; Kobilka, B. K. *EMBO J.* **2009**, *28*, 3315.
(29) Dietz, M. S.; Hasse, D.; Ferraris, D. M.; Gohler, A.; Niemann, H. H.; Heilemann, M. *BMC Biophys.* **2013**, *6*, 6.
(30) Groulx, N.; McGuire, H.; Laprade, R.; Schwartz, J. L.; Blunck, R. *J. Biol. Chem.* **2011**, *286*, 42274.
(31) Penna, A.; Demuro, A.; Yeromin, A. V.; Zhang, S. L.; Safrina, O.; Parker, I.; Cahalan, M. D. *Nature* **2008**, *456*, 116.
(32) Hamm, H. E.; Meier, S. M.; Liao, G.; Preininger, A. M. *Protein Sci.* **2009**, *18*, 2326.
(33) Degtyarev, M. Y.; Spiegel, A. M.; Jones, T. L. *J. Biol. Chem.* **1994**, *269*, 30898.
(34) Park, P.; Sum, C. S.; Hampson, D. R.; Van Tol, H. H.; Wells, J. W. *Eur. J. Pharmacol.* **2001**, *421*, 11.
(35) Redka, D. S.; Heerklotz, H.; Wells, J. W. *Biochemistry* **2013**, *52*, 7405.
(36) Rasmussen, S. G. F.; DeVree, B. T.; Zou, Y.; Kruse, A. C.; Chung, K. Y.; Kobilka, T. S.; Thian, F. S.; Chae, P. S.; Pardon, E.; Calinski, D.; Mathiesen, J. M.; Shah, S. T. A.; Lyons, J. A.; Caffrey, M.; Gellman, S. H.; Steyaert, J.; Skiniotis, G.; Weis, W. I.; Sunahara, R. K.; Kobilka, B. K. *Nature* **2011**, *477*, 549.
(37) Bacia, K.; Petrášek, Z.; Schwille, P. *ChemPhysChem* **2012**, *13*, 1221.
(38) Foo, Y. H.; Naredi-Rainer, N.; Lamb, D. C.; Ahmed, S.; Wohland, T. *Biophys. J.* **2012**, *102*, 1174.
(39) Comar, W. D.; Schubert, S. M.; Jastrzebska, B.; Palczewski, K.; Smith, A. W. *J. Am. Chem. Soc.* **2014**, *136*, 8342.
(40) Raicu, V. *J. Biol. Phys.* **2007**, *33*, 109.
(41) Pathak, A.; Smih, F.; Galinier, M.; Verwaerde, P.; Rouet, P.; Philip-Couderc, P.; Montastruc, J. L.; Senard, J. M. *Int. J. Obes.* **2005**, *29*, 176.
(42) Ma, A. W.; Pawagi, A. B.; Wells, J. W. *Biochem. Biophys. Res. Commun.* **2008**, *374*, 128.
(43) Seewöster, T.; Lehmann, J. *Biotechnol. Bioeng.* **1997**, *55*, 793.
(44) Bharill, S.; Fu, Z.; Palty, R.; Isacoff, E. Y. *Proc. Natl. Acad. Sci. U. S. A.* **2014**, *111*, 6491.
(45) Craggs, T. D. *Chem. Soc. Rev.* **2009**, *38*, 2865.
(46) Joo, C.; Ha, T. *Cold Spring Harbor Protocols* **2012**, *2012*, 071548.
(47) Heitz, F.; McClue, S. J.; Harris, B. A.; Guenet, C. *J. Recept. Signal Transduction Res.* **1995**, *15*, 55.
(48) Kusunoki, H.; Wakamatsu, K.; Sato, K.; Miyazawa, T.; Kohno, T. *Biochemistry* **1998**, *37*, 4782.
(49) Bommakanti, R. K.; Vinayak, S.; Simonds, W. F. *J. Biol. Chem.* **2000**, *275*, 38870.
(50) Coleman, D. E.; Berghuis, A. M.; Lee, E.; Linder, M. E.; Gilman, A. G.; Sprang, S. R. *Science* **1994**, *265*, 1405.
(51) Angers, S.; Salahpour, A.; Joly, E.; Hilairet, S.; Chelsky, D.; Dennis, M.; Bouvier, M. *Proc. Natl. Acad. Sci. U. S. A.* **2000**, *97*, 3684.

DOI: 10.1021/jacs.6b04032
J. Am. Chem. Soc. 2016, 138, 11583−11598

(52) Cottet, M.; Faklaris, O.; Maurel, D.; Scholler, P.; Doumazane, E.; Trinquet, E.; Pin, J. P.; Durroux, T. *Front. Endocrinol. (Lausanne, Switz.)* **2012**, *3*, 92.
(53) Jahangeer, S.; Rodbell, M. *Proc. Natl. Acad. Sci. U. S. A.* **1993**, *90*, 8782.
(54) Chidiac, P.; Wells, J. W. *Biochemistry* **1992**, *31*, 10908.
(55) Yang, J.; Chen, H.; Vlahov, I. R.; Cheng, J. X.; Low, P. S. *Proc. Natl. Acad. Sci. U. S. A.* **2006**, *103*, 13872.
(56) Higashijima, T.; Uzu, S.; Nakajima, T.; Ross, E. M. *J. Biol. Chem.* **1988**, *263*, 6491.
(57) Guo, W.; Shi, L.; Filizola, M.; Weinstein, H.; Javitch, J. A. *Proc. Natl. Acad. Sci. U. S. A.* **2005**, *102*, 17495.
(58) Hu, J.; Hu, K.; Liu, T.; Stern, M. K.; Mistry, R.; Challiss, R. A. J.; Costanzi, S.; Wess, J. *J. Biol. Chem.* **2013**, *288*, 34777.
(59) Kota, P.; Reeves, P. J.; Rajbhandary, U. L.; Khorana, H. G. *Proc. Natl. Acad. Sci. U. S. A.* **2006**, *103*, 3054.
(60) Davies, A.; Gowen, B. E.; Krebs, A. M.; Schertler, G. F. X.; Saibil, H. R. *J. Mol. Biol.* **2001**, *314*, 455.
(61) Jastrzebska, B.; Chen, Y.; Orban, T.; Jin, H.; Hofmann, L.; Palczewski, K. *J. Biol. Chem.* **2015**, *290*, 25728.
(62) Bokoch, G. M.; Katada, T.; Northup, J. K.; Ui, M.; Gilman, A. G. *J. Biol. Chem.* **1984**, *259*, 3560.
(63) Jastrzebska, B.; Ringler, P.; Lodowski, D. T.; Moiseenkova-Bell, V.; Golczak, M.; Müller, S. A.; Palczewski, K.; Engel, A. *J. Struct. Biol.* **2011**, *176*, 387.
(64) Banères, J.-L.; Parello, J. *J. Mol. Biol.* **2003**, *329*, 815.
(65) Wang, J.; Sengupta, P.; Guo, Y.; Golebiewska, U.; Scarlata, S. *J. Biol. Chem.* **2009**, *284*, 16906.
(66) Nenasheva, T. A.; Neary, M.; Mashanov, G. I.; Birdsall, N. J.; Breckenridge, R. A.; Molloy, J. E. *J. Mol. Cell. Cardiol.* **2013**, *57*, 129.
(67) Mazouchi, A.; Liu, B.; Bahram, A.; Gradinaru, C. C. *Anal. Chim. Acta* **2011**, *688*, 61.
(68) Banks, D. S.; Fradin, C. *Biophys. J.* **2005**, *89*, 2960.
(69) Bacia, K.; Schwille, P. *Nat. Protoc.* **2007**, *2*, 2842.
(70) Raicu, V.; Stoneman, M. R.; Fung, R.; Melnichuk, M.; Jansma, D. B.; Pisterzi, L. F.; Rath, S.; Fox, M.; Wells, J. W.; Saldin, D. K. *Nat. Photonics* **2009**, *3*, 107.
(71) Jain, A.; Liu, R.; Xiang, Y. K.; Ha, T. *Nat. Protoc.* **2012**, *7*, 445.
(72) Liu, B.; Mazouchi, A.; Gradinaru, C. C. *J. Phys. Chem. B* **2010**, *114*, 15191.
(73) Watkins, L. P.; Yang, H. *J. Phys. Chem. B* **2005**, *109*, 617.
(74) Berendsen, H. J. C.; Vanderspoel, D.; Vandrunen, R. *Comput. Phys. Commun.* **1995**, *91*, 43.
(75) Lindahl, E.; Hess, B.; van der Spoel, D. *J. Mol. Model.* **2001**, *7*, 306.
(76) Shinobu, A.; Palm, G. J.; Schierbeek, A. J.; Agmon, N. *J. Am. Chem. Soc.* **2010**, *132*, 11093.

DOI: 10.1021/jacs.6b04032
J. Am. Chem. Soc. 2016, 138, 11583−11598